UCR/IGPP--83/7

DE83 016724

CALC-SILICATE MINERALIZATION IN ACTIVE GEOTHERMAL SYSTEMS

Dennis K. Bird

Department of Geology

Stanford University

Stanford, CA 94305

and

Peter Schiffman, Wilfred A. Elders and Alan E. Williams

Institute of Geophysics and Planetary Physics

University of California

Riverside, CA 92521

and

AC07-80ID12145

S. Douglas McDowell

Department of Geology and Geological Engineering

Michigan Technological University

Houghton, MI 49931

DISCLAIMER

ABSTRACT

Calc-silicates in the system $CaO-FeO-MgO-Fe_2O_3-Al_2O_3-TiO_2-SiO_2-H_2O$ are an important group of rock-forming minerals found in drillhole samples from active geothermal areas worldwide. The most common metasomatic calc-silicates in geothermal systems are heulandite, laumontite, wairakite, prehnite, epidote, garnet, sphene, clinopyroxene, actinolite, and wollastonite. Conditions of temperature, pressure, and the chemical characteristics of hydrothermal fluids associated with the occurrence of these minerals can be readily obtained from drillhole measurements. Observations such as these allow critical evaluation of the relationships between intensive thermodynamic properties and phase relationships of calc-silicates in active magma-hydrothermal systems.

A distinct sequence of calc-silicates is found which, in general, reflects progressive dehydration with increasing temperature. Heulandite and laumontite usually occur at temperatures below 200°C, whereas wairakite, epidote, prehnite, and actinolite occur within the range of temperatures from 200°C to greater than 300°C. Anhydrous phases of garnet, clinopyroxene, and wollastonite typically are found at temperatures greater than 300°C. With the exception of laumontite and wollastonite, hydrothermal calc-silicates exhibit a diverse range of compositions. Alkalis substitute for calcium in heulandite and wairakite, and there is considerable octahedral substitution of ferric iron for aluminum in epidotes, prehnite, and garnet and of ferrous iron for magnesium in clinopyroxenes and actinolites. In some cases it can be shown that coexisting compositions of epidote and garnet, and actinolite and clinopyroxene represent nonequilibrium partitioning of octahedral cations when compared with experimental, theoretical, and natural metamorphic phase relations.

In the Cerro Prieto and Salton Sea geothermal systems there are subtle systematic gradients in the averaged compositions of epidotes with increasing depth and temperature. Discontinuities in these compositional gradients are

closely associated with the appearance or disappearance of one or more of the phases calcite, prehnite, wairakite, or biotite. From the available data there is no other obvious systematic correlation between observed compositional trends of calc-silicates and either depth or temperature in most geothermal systems. Bulk rock and fluid compositions appear to be important factors controlling the observed compositional characteristics of these minerals.

Our detailed study of calc-silicate mineral zones and coexisting phase relations in the Cerro Prieto geothermal system were used as examples for thermodynamic evaluation of phase relations among minerals of variable composition and to calculate the chemical characteristics of hydrothermal solutions compatible with the observed calc-silicate assemblages. In general there is a close correlation between calculated and observed fluid compositions. Calculated fugacities of O_2 at about 320°C in the Cerro Prieto geothermal system are about five orders of magnitude less than that at the nearby Salton Sea geothermal system. This observation is consistent with the occurrence of Fe^{3+} rich epidotes in the latter system and the presence of prehnite at Cerro Prieto.

INTRODUCTION

Mineral assemblages containing calc-silicates are characteristic of a wide variety of geologic environments in the earth's crust. Phase relations and zoning patterns of calc-silicates are widely used to discriminate regional metamorphic facies, and as an exploration tool in many mining districts. In fossil magma-hydrothermal systems metasomatic mineral zoning of calc-silicates is commonly found both within the intrusive heat source and in its host rocks, where dramatic chemical potential gradients can be inferred from outcrop relations. However in metamorphic terranes and fossil magma-hydrothermal systems the intensive thermodynamic variables responsible for the observed calc-silicate mineral assemblages cannot be directly measured. Consequently, temperatures, pressures,

and the chemical potentials of thermodynamic components must be predicted or inferred from experimental data, thermodynamic analysis of phase relations, isotopic compositions of coexisting phases, stratigraphic reconstructions, or fluid inclusion analyses. Detailed studies of calc-silicate mineralization in modern geothermal systems does allow correlation of mineral compatibilities with measured temperatures, pressures, and coexisting fluid compositions determined from measurements and sampling in deep drill holes. Such observations are critical to evaluating calc-silicate phase relations in geologic systems as they provide a unique test of predictive methods for estimating the intensive thermodynamic variables associated with comparable paleogeologic processes.

In the past twenty years exploration of geothermal systems for electric power production has provided detailed information on hydrothermal mineral assemblages in deep drill holes. Unfortunately much of the data are proprietary or have been reported in "in-house" publications and symposium volumes with restricted circulation. A review paper by Browne (1978) summarized the occurrence and distribution of hydrothermal minerals in several geothermal systems. However, to date there has been no current compilation of the vast data base of compositional relations among these authigenic minerals.

The purpose of this paper is to summarize the distributions, occurrences, compositional characteristics, and thermodynamic relations of calc-silicates in explored geothermal systems. This group of minerals includes calcium silicates in the system CaO-FeO-Fe_2O_3-Al_2O_3-TiO_2-MgO-SiO_2-H_2O. In our study we have placed particular emphasis on the dramatic metasomatic mineral zoning of calc-silicates in the extensively drilled Cerro Prieto geothermal system of Baja California. We have calculated theoretical phase diagrams accounting for compositional variation and substitutional order/disorder in these calc-silicates and compared them with the observed fluid and mineral compatibilities at measured temperatures and pressures in deep drill holes.

CALC-SILICATE MINERALS IN GEOTHERMAL SYSTEMS

Metasomatic calc-silicates reported in cores and cuttings of geothermal drill hole samples include framework silicates (calcium-zeolites), single chain silicates (wollastonite and calcium clinopyroxenes), double chain silicates (actinolitic amphiboles), sheet silicates (prehnite), orthosilicates (garnet and sphene), and orthosorosilicates (epidote). For reference, the stoichiometric endmember compositions of the calc-silicates commonly occurring in geothermal fields are depicted in Figure 1. In general the hydrous phases, containing either structural or zeolitic water, are the most abundant calc-silicates in geothermal systems. Anhydrous phases including garnet, pyroxene, and wollastonite are typically restricted in their distribution and abundance to the deeper-higher temperature portions thus far explored by drilling in active geothermal systems. Very few geothermal calc-silicates correspond to the stoichiometric analogs shown in Figure 1. Highly variable solid solutions are typical of the minerals found in active geothermal systems.

The documented occurrences of calc-silicate minerals in worldwide active geothermal systems are presented in Table 1. These minerals have crystallized within reservoirs of greatly differing protoliths (i.e., volcanic, sedimentary, metamorphic) and brine composition (i.e., total dissolved solids, pH, etc.). The modes of occurrence, distributions, and compositional variations of specific calc-silicate minerals in active geothermal systems are outlined below. Details concerning the occurrence and composition of these minerals in the Cerro Prieto system are presented in a later section.

Calcium Zeolites

Zeolites occur in virtually every major geothermal system in the world (Table 1). In addition to the more common phases (heulandite, laumontite, and wairakite), other calcium zeolites which have been reported from active geothermal systems include stilbite, chabazite, thomsonite, scolecite, mordenite,

yugawaralite, levyne, gismondine, and gmelinite (Browne, 1978; Kristmannsdottir and Tomasson, 1976).

The calcium zeolites, with the notable exception of wairakite, generally are found in the lower temperature (i.e., <200°C) portions of active geothermal systems. Three different fabrics that typify their occurrence are: (1) within fractures and vesicles; (2) as selective replacement products of relict feldspars; and (3) as recrystallization products of the glassy or calcareous/siliceous matrix of volcanic, tuffaceous, or sedimentary rocks.

The only appreciable chemical variation in geothermal calcium-zeolites is partial replacement of Ca^{++} by Na^{+} or K^{+}, and Si^{4+} for Al^{3+} which is required to maintain charge balance. To date there have been no analyses of the content of zeolitic water in the natural occurring geothermal zeolites. Measured compositions of heulandite, laumontite, and wairakite reported from active geothermal systems are shown in Figure 2. The high alkali content of heulandite shown in the figure is probably due to the alkali-rich rhyolitic flows, tuffs, and epiclastic sediments which make up the Yellowstone geothermal reservoirs rocks. In contrast to heulandite, the composition of geothermal laumontite is nearly stoichiometric, with less than 5 mole % Na+K.

Wairakite is probably the most common Ca-zeolite in geothermal systems and also one of the few zeolites whose occurrence is largely restricted to geothermal systems, active or fossil. In many active geothermal systems, wairakites have crystallized to temperatures in excess of 200°C, and often coexist with epidote. Geothermal wairakites exhibit considerable solid solution with up to 40 mole % of the analcime component for the Yellowstone analyses. The reservoir rock composition appears to exert some constraints on the Ca/Na contents of geothermal wairakites; wairakites recrystallized in basic to intermediate volcanic rock reservoirs (e.g., diabasic dikes in the Heber field and andesites in

Otake and Onikobe) are generally more calcic than those recrystallized in silicic reservoir rocks (e.g., rhyolites of Yellowstone and Wairakei).

Prehnite

Prehnite has been reported from several active geothermal systems (Table 1) in which it appears to have formed at temperatures between 250° and 350°C. The occurrence of prehnite is generally restricted to systems containing basic volcanic rocks (e.g., Iceland, Heber, Kamchatka) or calcareous metasediments (e.g., Larderello, The Geysers, Cerro Prieto). In these systems, prehnite typically occurs as a vein or amygdaloidal mineral, although it has been reported as an alteration product of primary plagioclase and ferro-magnesium minerals (e.g., Heber and Wairakei) and as a cementing material in tuffaceous (e.g., Wairakei) and sedimentary (e.g, Cerro Prieto) rocks.

As with metamorphic prehnites, the major deviations from stoichiometry results from octahedral substitution of Fe^{3+} for Al^{3+} (Fig. 3). The prehnites from diabasic dikes in the Heber field exhibit the largest $Fe/Fe+Al^{VI}$ variations (0.01-0.27). From these data there is no apparent correlation between temperature and prehnite compositon.

Epidote

Aside from the zeolites, epidote is the calc-silicate mineral most commonly reported from active geothermal systems. In fact, epidote has been reported from virtually every geothermal system in which temperatures exceed approximately 250°C (Table 1). In addition, once epidote is encountered in the metamorphic mineral stratigraphy of an individual well, it generally remains as the dominant calc-silicate phase throughout the remainder of the well.

Like prehnite, the major nonstoichiometry of epidote solid solutions results from the substitutions of Fe^{3+} and Al^{3+} in the octahedral sites. Epidotes from active geothermal systems are commonly zoned and may exhibit wide compositional variations both within individual grains (e.g., PS 27-38 for an

epidote in Magmamax 2 of the Salton Sea field [Tewhey, 1977] and PS 18-31 for an epidote in Profondo from Larderello [Cavarretta et al., 1982]) and between grains from a single geothermal field (e.g., PS 12-37 for epidotes in Sasso 22 of the Larderello field; ibid)[1]. The $Fe/Fe+Al^{VI}$ contents of epidotes from five geothermal systems (Figure 3) ranges from PS 11-40. There is no indication of an epidote immiscibility gap as proposed by Strens (1965) and Raith (1976) from their observations of regional metamorphic rocks.

Epidote compositions from most geothermal systems show no obvious correlation of pistacite content with depth or temperature. However, the pistacite content of epidotes in Elmore #1 of the Salton Sea geothermal field (McDowell and McCurry, 1978; McDowell and Elders, in preparation) increases abruptly from PS 19 to PS 29 at temperatures near 325°C. This temperature corresponds to the first formation of biotite and the last occurrence of calcite with increasing depth and temperature in the well. The pistacite content then gradually decreases on increasing temperature where epidote coexists with biotite. The most Fe-rich epidotes reported from an active geothermal system are those from the diabasic dikes in the Heber field (Browne, 1977). The high Fe-content of these epidotes corresponds to similarly high Fe-contents of the coexisting prehnite (Figure 3).

Actinolite

Amphiboles of the tremolite-actinolite solid solution series have been reported from several active geothermal systems at temperatures exceeding ~250°C or more commonly 300°C. Amphiboles in geothermal systems typically occur as very fine-grained acicular crystals either in felted aggregates (sub-parallel to randomly-oriented) or spherulitic-type clusters, partially filling uncemented pores (of sandstones) or included within other phases (e.g., feldspars or clinopyroxenes).

[1] PS denotes the mole fraction of $Ca_2Fe_3Si_3O_{12}(OH)$ in epidote solid solutions.

Compositionally, all authigenic amphiboles reported from active geothermal systems are low - Al_2O_3 (<2.5 wt %, but generally <1.0 wt % and dominantly octahedrally coordinated), low - Na_2O (<0.5 wt % and dominantly occupying M4 sites) members of the tremolite-actinolite series, with Mg/Mg+Fe+Mn ratios ranging from .45-.82. Although the existing data are scant, the available analyses (Figure 4) cluster into two compositional fields: Mg/Mg+Fe+Mn ratios of approximately 80% and 50%.

Clinopyroxenes

Clinopyroxenes in active geothermal systems are found at >300°C and have distinctive crystal habits which are generally unlike those observed in other metamorphic rocks such as skarns, calc-silicate hornfels, or granulites. Clinopyroxenes from the Larderello geothermal system (Cavarretta et al., 1982) occur in cavities and fractures and form "turbid microcrystalline masses and radiating to fan-shaped aggregates."

The limited compositional data on clinopyroxenes from active geothermal systems are shown in Figure 4. All of these clinopyroxenes are high-calcium augites with very minor "other than quadrilateral" components. Mg/Mg+Fe+Mn contents range from 0.0 to 0.80. Clinopyroxenes from IID #2 of the Salton Sea geothermal field (McDowell, unpublished data, 1982) cluster into two compositionally distinct groups: augite with Mg/Mg+Fe+Mn from 0.6-0.8 and nearly pure hedenbergite with significant octahedrally coordinated Mn.

Garnets

Garnets have been reported from six active geothermal systems (Table 1). These garnets apparently form at temperatures generally exceeding 300°C. The garnets typically occur as fine-grained idioblasts, filling veins and pores in association with epidote, clinopyroxene, or more rarely, wollastonite. Compositionally, the garnets are dominantly andradite with less than 35 mole % grossularite component (Figure 4); pyralspite comprises less than 5 mole %.

McDowell and Elders (in preparation) have described zoned titaniferrous andradites from the Salton Sea field.

Wollastonite

Wollastonite has been described from only three active geothermal systems (Table 1): Krafla, Iceland (Kristmannsdottir, 1981); Tongonan, Philippines (Ferrer, 1983); and Larderello, Italy (Cavarretta et al., 1982). In all of these localities, the wollastonite forms as fibrous or bladed crystals often in fan-shaped aggregates. In the Krafla geothermal field, wollastonite is found at depths (600-1500 m) for which present temperatures range from 200-340°C. In the lower-temperature (i.e., <300°C) occurrences, the wollastonite occurs solely in "contact metamorphic" veins filled with andradite, hypersthene, and magnetite. The development of these veins is believed to be related to dike emplacement (Kristmannsdottir, 1981). The occurrence of wollastonite at higher temperatures appears to be unrelated to local dike emplacement as determined from available well log data. In the Tongonan geothermal field (Ferrer, 1983), wollastonite occurs within a metacarbonate skarn assemblage also containing andradite, calcite, and anhydrite. Maximum measured downhole temperatures in the wollastonite-bearing well are 284°C and no intrusive bodies were reported.

Other Calc-Silicates

Titanite (sphene) has been reported from several active geothermal systems (Table 1) in which it occurs in very fine-grained, generally granular aggregates.

Datolite has been described from several wells in the Larderello geothermal system (Cavarretta et al., 1982) where it occurs as large xenoblasts in association with many of the higher temperature calc-silicate minerals previously described. Datolite has also been identified in calcite veins cutting metagreywacke in The Geysers (Moore, personal communication).

Idocrase has been reported from a metacarbonate skarn in the Tongonan geothermal field (Ferrer, 1983) in which it is associated with wollastonite and garnet (see previous section).

Pumpellyite has been reported from the Reykjavik and Hveragerdi geothermal fields of Iceland (Sigvaldeson, 1962). However, the pumpellyite in these relatively low-temperature systems probably is a relict from a previous, possibly ocean-floor metamorphic, period of hydrothermal alteration (Seki, 1972).

Calc-Silicate Mineral Zoning

The calc-silicate minerals of active geothermal systems are commonly found in a temperature/depth related zonation. Representative examples of such mineral zonations in four active geothermal fields are given in Figure 5. Although existing downhole temperature-depth profiles may not accurately reflect the conditions under which these calc-silicate minerals have crystallized, Figure 5 depicts some obvious relationships between measured temperatures and the spacial distributions of calc-silicates.

These relationships are summarized in Figure 6 for all available data from geothermal systems listed in Table 1. The calcium zeolites, exclusive of wairakite, are restricted to temperatures <200°C; wairakite occurs to temperatures of 250°C to slightly greater than 300°C. The lower temperature occurrences of prehnite, epidote, and possibly ferroactinolite overlap with wairakite. Occurrences of clinopyroxene, garnet, and wollastonite are predominantly restricted to temperatures >300°C. With the exception of the zeolites, all of the above-described calc-silicates can occur in the highest temperature (300° to approximately 375°C) portions of active geothermal systems.

The mineral zoning with increasing depth and temperature reflects progressive dehydration of calc-silicate minerals. In general this is shown by Figure 1 where, with increasing temperatures, the amount of zeolitic or

structural water in the stable calc-silicate assemblage decreases. The notable exception to this is apparent in the epidote-prehnite phase relations given in Figure 6, where epidote is found to occur at lower temperatures than prehnite. This relationship is a consequence of difference in Fe^{3+} solubility in the octahedral sites of prehnite and epidote solid solutions. The maximum octahedral substitution of Fe^{3+} for Al^{3+} in the octahedral sites of geothermal epidotes is ~1.2 moles of Fe^{3+} per mole of epidote, whereas geothermal prehnites have <0.3 moles of Fe^{3+} per moles of prehnite (Figure 3). The increased substitution of octahedral Fe^{3+} in epidote increases its stability field to lower temperatures and decreases the relative stability of coexisting prehnite (Bird and Helgeson, 1981; also see Figure 19 below).

EQUILIBRIUM PHASE RELATIONS

An understanding of equilibrium phase relations among aqueous solutions and calc-silicates is essential for adequate description and interpretation of metasomatic mineral zoning and chemical mass transfer in geothermal systems. Calculated phase diagrams illustrating the dependence of temperature, pressure, and the activities of aqueous species on the stability relations of calc-silicates are summarized below for conditions typical of active geothermal systems. As noted above, a wide range of compositional variation and substitutional order-disorder exists in natural calc-silicate minerals in active geothermal systems. Consequently, stoichiometric phase relations are summarized so as to provide a frame of reference for considering the consequences of natural occurring mineral assemblages.

Stoichiometric Mineral Relations

Univariant phase relations of minerals in the system CaO-Al_2O_3-SiO_2-H_2O in the presence of quartz and an aqueous solution with $a_{H_2O} \sim 1$ have recently been reported by Bird and Helgeson (1981) and Hammerstrom and Brown (1983). For temperatures and pressures commonly observed in geothermal reservoirs,

which are close to the saturation curve for H_2O, there is a distinct zoning in the predicted stability relations of calc-silicate minerals. For example, in the presence of aqueous solutions that are close to equilibrium with α-quartz, heulandite is stable between ~110° and 180°C, wairakite is stable to temperatures ≲360°C and clinozoisite and grossular are stable at temperatures greater than ~230° and 320°C, respectively.

The temperature dependence of log $\underline{a}_{Ca^{++}}/\underline{a}^2_{H^+}$ in an aqueous solution coexisting with calcium-aluminum-silicates are depicted in Figures 7a and 7b for equilibrium with either quartz or amorphous silica. Comparison of these figures illustrates the extreme dependence of mineral phase relations on the concentration of $SiO_{2(\underline{aq})}$ in the fluid phase (also see Figures 8a and 8b). Note that the range in fluid composition coexisting with calcium-aluminum-silicates at constant temperature is restricted to ≲3 orders of magnitude in the value of $\underline{a}_{Ca^{++}}/\underline{a}^2_{H^+}$ in the fluid phase, and that $\underline{a}_{Ca^{++}}/\underline{a}^2_{H^+}$ decreases with increasing temperature for calcium-aluminum-silicate mineral assemblages. The latter observation is a consequence of the negative standard molal enthalpies for hydrolysis reactions that depict the phase boundaries in Figure 7.

It is apparent from Figure 8 that the Ca-zeolites, laumontite and wairakite can coexist only with an aqueous solution in which $\underline{m}_{SiO_{2(aq)}}$ ($\sim a_{SiO_{2(aq)}}$) is approximately equal to or greater than that for saturation with α-quartz, but that clinozoisite is constrained to aqueous solutions in which $\underline{m}_{SiO_{2(aq)}}$ is less than that for saturation with amorphous silica. Also note that the range in values of the ratio of $a_{Ca^{++}}/a^2_{H^+}$ in the aqueous phase coexisting with the clinozoisite or margarite decreases dramatically with increasing concentration of $SiO_{2(aq)}$ above that equivalent to saturation with α-quartz.

Phase relations among minerals in the system K_2O-Na_2O-CaO-Al_2O_3-SiO_2-H_2O-HCL in the presence of quartz and an aqueous phase in which a_{H_2O} are shown in Figures 8c through 8f as a function of log $\underline{a}_{Ca^{++}}/\underline{a}^2_{H^+}$ and either log $\underline{a}_{Na^+}/\underline{a}_{H^+}$ or

log a_{K^+}/a_{H^+} in the coexisting aqueous phase for 200° and 300°C and pressures corresponding to the liquid-vapor equilibrium of H_2O. These figures illustrate equilibrium phase relations among calcium-aluminum-silicates and the important rock forming geothermal minerals albite, K-feldspar and muscovite. As a consequence of increasing temperature, the values of $\underline{a}_{Ca^{++}}/\underline{a}^2_{H^+}$, $\underline{a}_{Na^+}/\underline{a}_{H^+}$, and $\underline{a}_{K^+}/\underline{a}_{H^+}$ compatible with hydrous alumino-silicates decrease in accord with the relative increase of the stability of the anhydrous minerals shown in the figure. Although clinozoisite is stable in the presence of an aqueous solution and quartz at temperatures of 250° and 300°C (Figures 7a and 8d), it can be seen in Figure 8d that K-feldspar is not compatible with the assemblage clinozoisite+quartz+ aqueous solution. This is the result of the intravening fluid compositions in equilibrium with muscovite. At temperature greater than ~320°C, the assemblage of stoichiometric K-feldspar+clinozoisite+quartz is stable in the presence of an aqueous solution.

Although this observation appears to contravene geologic observations of coexisting epidote solid solutions and potassium-feldspars within active geothermal systems such as Wairakei (Steiner, 1958), Salton Sea (Keith, Muffler and Cremer, 1968; Kendall, 1976; McDowell and Elders, in preparation), Otake (Hayashi and Yamasaki, 1976), and Cerro Prieto (Elders et al., 1981), it has been shown by Bird and Helgeson (1980) that Fe^{3+} substitution for Al^{3+} in clinozoisite to form epidote solid solutions decreases dramatically the minimum temperature compatible with the assemblage. Compositional variation and substitutional order/disorder in epidote solid solution must be explicitly accounted for in thermodynamic calculations in order to obtain consistency among the observed and calculated pressures, temperatures, and phase relations reported in these geothermal areas. This observation underscores the important role nonstoichiometry and order/disorder in minerals partake in measured phase relations and fluid compositions in active geothermal systems.

Phase relations among minerals in the system $CaO-MgO-SiO_2-H_2O$ are given in Figure 9, together with phase compatibilities of calcium-aluminum-silicates in the presence of quartz and an aqueous solution. Note that the activity ratio of Ca^{++} to Mg^{++} cations in an aqueous solution coexisting with quartz and either wollastonite+diopside, diopside+tremolite, or tremolite+talc decreases with increasing temperature as a consequence of the negative standard molal enthalpy of reactions describing these divariant mineral assemblages. It can be seen in Figure 9 that stoichiometric diopside is not stable with clinozoisite at any temperature <350°C along the saturation curve for H_2O. It will be shown below that nonstoichiometry in these minerals to form epidote and calcium clinopyroxene solid solutions permits their stable coexistence at temperatures <350°C in active geothermal systems.

Activity-Composition Relations

Thermodynamic analysis of phase relations involving naturally occurring calc-silicates of variable composition requires explicit provision for the substitution of atoms on energetically equivalent sites, as well as the exchange of atoms among energetically distinct sites in the crystal lattice. In this study nonstoichiometry in minerals is accounted for by activity-composition relations for thermodynamic components of solid solutions summarized by Helgeson, Delany, Nesbitt and Bird (1978), Bird and Helgeson (1980), Helgeson and Aagaard (1983), and Bird and Norton (1981).

Equations and data describing activity composition relations for garnet, prehnite, and epidote solid solutions are given by Bird and Helgeson (1980). For the latter mineral the equations and data explicitly account for the temperature dependence of substitutional order/disorder of octahedral Al^{3+} and Fe^{3+}. In view of compositional and site occupancy uncertainties of tremolite solid solutions in geothermal systems and uncertainties in cation occupancy in natural tremolite solid solutions, we have assumed for the calculations presented below that

$$a_{Ca_2Mg_5Si_8O_{22}(OH)_2} \approx X_{Ca_2Mg_5Si_8O_{22}(OH)_2} \quad . \tag{1}$$

The standard state stoichiometry for diopside and hedenbergite adopted in this study is $(Ca)^{M2}(Mg)^{M1}Si_2O_6$ and $(Ca)^{M2}(Fe)^{M1}Si_2O_6$, respectively. The M2 site is normally completely occupied by Ca; Fe^{2+} and Mg reside in the smaller M1 sites. Nevertheless, there is evidence that small amounts of Fe^{2+} can occur in the M2 sites (Robinson, 1980). The distribution of Fe and Mg among the M1 and M2 sites can be described by the reaction

$$Fe^{M2} + Mg^{M1} \rightleftharpoons Fe^{M1} + Mg^{M2} \quad , \tag{2}$$

for which the mass action equation can be expressed as

$$K = \frac{X_{Fe,M1}X_{Mg,M2}}{X_{Fe,M2}X_{Mg,M1}} \tag{3}$$

which is consistent with random mixing and equal interaction of Fe^{2+} and Mg in the M1 and M2 sites.

Values of the equilibrium constant for reaction (4) have been determined by McCallister, Finger and Ohashi (1976). These values are consistent with slight ordering of Fe in the M2 site relative to Mg. This ordering apparently decreases with increasing temperature. In view of the available experimental data, the following site distributions are adopted for geothermal clinopyroxenes formed at temperatures less than 350°C:

(1) Ca is preferentially ordered in the M2 site.

(2) Fe^{2+} fills the remainder of the M2 site so that $X_{Ca,M2} + X_{Fe,M2} = 1$.

(3) The rest of the Fe and all the Mg are in the M1 site. These site distributions are consistent with the following activity-composition relations:

$$a_{CaMgSi_2O_6} = X_{Ca,M2}X_{Mg,M1}X^2_{Si,T} \tag{4}$$

and

$$a_{CaFeSi_2O_6} = X_{Ca,M2}X_{Fe,M1}X^2_{Si,T} \quad . \tag{5}$$

Partitioning of Octahedral Cations

Compositional relations among coexisting minerals in geothermal systems allows evaluation of the partitioning of octahedral Fe^{3+} and Al^{3+} among epidote, garnet and prehnite solid solutions, and Fe^{2+} and Mg^{2+} partitioning among coexisting pyroxene and tremolite solid solutions. Comparison of compositional relations among these minerals in geothermal systems with phase relations in other geologic environments and calculated equilibrium compositions are presented below.

Measured compositions of coexisting epidote and garnet solid solutions from the Salton Sea, Geysers, and Larderello geothermal fields are given in Figure 10. For comparison the range of measured compositions of these minerals from contact skarn deposits and calculated equilibrium partitioning of Fe^{3+} and Al^{3+} are also shown in the figure. With the exception of the analyses reported by Kendall (1976) all the geothermal garnets coexisting with epidotes are close to andradite in composition. The available experimental (Holdaway, 1972; Liou, 1973) and theoretical (Bird and Helgeson, 1980) observations indicate that these andradite garnet-epidote assemblages do not represent equilibrium assemblages. Similar compositional relations among andradite rich garnets and intermediate epidote (PS 10 to 30) have been reported in low grade regional metamorphic rocks (Coombs et al., 1977), skarns (Kwak, 1978), and hydrothermal veins in the Skaargard intrusion (D. K. Bird, unpublished data, 1981).

Equilibrium between coexisting epidote and prehnite solid solutions can be represented by the law of mass action for the reaction

$$Ca_2FeAl_2Si_3O_{12}(OH) + Ca_2Al(AlSi_3O_{10})(OH)_2 \rightleftharpoons Ca_2Al_3Si_3O_{12}(OH) + Ca_2Fe(AlSi_3O_{10})(OH)_2. \quad (6)$$

Taking into account the activity-composition relations adopted above for the thermodynamic components of epidote and prehnite solid solutions allows us to write

$$X_{Al,M,Ca_2Al(AlSi_3O_{10})(OH)_2} = \left(1 + K_{T,P}\left[\frac{a_{Ca_2FeAlSi_3O_{12}(OH)}}{a_{Ca_2Al_3Si_3O_{12}(OH)}}\right]\right)^{-1} \quad (7)$$

where $K_{T,P}$ is the equilibrium constant for reaction (6) at the subscripted temperature and pressure and $X_{Al,M,Ca_2Al(AlSi_3O_{10})(OH)_2}$ is the mole fraction of octahedral aluminum in prehnite solid solutions coexisting with an epidote solid solution with a composition consistent with the activities specified for the $Ca_2FeAlSi_3O_{12}(OH)$ (epidote) and $Ca_2Al_3Si_3O_{12}(OH)$ (clinozoisite) thermodynamic components. Measured compositions of contiguous epidote and prehnite solid solution minerals from sandstones in the Cerro Prieto geothermal system (Figure 11) are consistent with an equilibrium constant for reaction (6) at approximately 300° to 320°C and pressures of 85 to 115 bars of $\sim 10^{-1.27}$. Note that this value is also in close agreement with measured compositions of epidote and prehnite solid solutions from hydrothermal veins near the Skaergärd intrusion of East Greenland and in metabasites from the Del Puerto ophiolite (Schiffman, 1978).

There is very limited data on the compositions of coexisting clinopyroxenes and amphiboles in active geothermal systems. Average analyses reported by Cavarretta et al. (1982) for the Larderello-Travale geothermal field indicate that the mole fraction of octahedral Mg^{++} is ~0.82 and ~0.91 for actinolites and clinopyroxenes, respectively. These analyses are close to the ideal fractionation reported by Mueller (1961) for metamorphic mineral assemblages. However, analyses from the Cerro Prieto geothermal system (Table 2 below, well M93, 2424 m) are significantly different, with mole fractions of octahedral Mg^{++} being ~0.73 and ~0.37 respectively for actinolite and clinopyroxene. In view of the available data from metamorphic systems and thermodynamic considerations reported by Ghose and Ganguly (1982) it is highly likely that the actinolite-

pyroxene assemblage observed at Cerro Prieto does not represent an equilibrium fractionation of Fe^{++} and Mg^{++} among these minerals.

Phase diagrams accounting for compositional variation and substitutional order/disorder in minerals consistent with the equations and data given above are presented below in the analysis of fluid and mineral compatibilities in the Cerro Prieto geothermal system.

CALC-SILICATE MINERALIZATION IN THE CERRO PRIETO GEOTHERMAL FIELD

The Cerro Prieto geothermal field (Figure 12), 28 km southeast of Mexicali, Mexico, lies within the delta of the Colorado River at the head of the Gulf of California. Since the Pliocene or late Miocene (Muffler and White, 1969; Van de Kamp, 1973), terrigenous sediments of the Colorado River have been deposited into a broad structural basin of the Salton Trough. Like the Gulf of California, the Salton Trough is a tectonic regime characterized by high regional heat flow, recurrent seismicity, and active volcanism (Elders, 1979).

Stratigraphic thicknesses of deltaic sediments in the Salton Trough are believed to approach 6 km (Muffler and Doe, 1968). A recent seismic study (Fuis et al., 1982) indicates a two-layer regional crustal structure: an upper section, approximately 5 km thick whose seismic properties (V_p = 2 to 5.6 km/sec) are compatible with unmetamorphosed sediments, and a 10 km deeper section characterized by a constant V_p = 5.65 km/sec, compatible with metamorphosed sediments. In the Cerro Prieto geothermal field, wells in excess of 3 km have not reached basement.

Compositionally, unmetamorphosed sediments at the Cerro Prieto geothermal field are similar to modern deltaic Colorado River sediments (Muffler and Doe, 1968) and to other unmetamorphosed sediments of the Salton Trough (Van de Kamp, 1973); these largely consist of continentally-derived sandstones, siltstones, and mudstones. Mineralogically, these sediments are predominantly comprised of

quartz and feldspar with subordinate amounts of carbonate (both calcite and dolomite) and clays (illite, montmorillonite, and kaolinite), and minor abundances of heavy minerals and detrital phyllosilicates (i.e., muscovite, biotite, and chlorite); lithic fragments (predominantly chert and volcanic) are also minor components (see Table 1 of Van de Kamp, 1973).

Within the geothermal field, these deltaic sediments have undergone systematic changes in mineralogy and texture due to interaction with geothermal fluids at elevated temperatures. Elders et al. (1979, 1981) have recognized four hydrothermal mineral zones believed to have formed in response to post-depositional, hydrothermal alteration. In order of increasing depth/temperature, these zones are: (1) the montmorillonite-kaolinite zone (<150° to 180°C), consisting of detrital and diagnetic-kaolinite and/or montmorillonite±dolomite±interlayered illite/montmorillonite; (2) the illite-chlorite zone (150° to 180°C through 230° to 250°C), characterized by a decrease in montmorillonite and kaolinite and an increase in illite and chlorite; (3) the calc-aluminum silicate zone (230° to 250°C through >350°C), characterized by the development of a variety of calc-silicate phases including epidote, wairakite, prehnite, actinolite and calcium clinopyroxene which co-exist with chlorite and illite; and (4) an overlapping biotite zone (315° to 325°C through >350°C), characterized by the development of authigenic biotite as the predominant phyllosilicate which co-exists with the higher temperature calc-silicates (i.e., epidote, actinolite, and calcium clinopyroxene).

Textural variations through these mineralogic zones are largely restricted to the pore-filling cement. Framework grains undergo some resorption or overgrowth and matrix phyllosilicates are progressively recrystallized, but the major textural and mineralogic modification of these sediments occurs in the pore-filling cement and in fractures. Near the top of the geothermal field, the unconsolidated clastic sediments have become indurated, largely because of the

development of a carbonate cement (or to a lesser extent, a siliceous or feldspathic cement). The precipitation of carbonate in the pores of these sediments is believed to occur as a consequence of the recharging of cold, HCO_3-rich waters into hotter portions of the system (Elders et al., 1979). These carbonate cemented sediments are the cap rocks to the geothermal reservoir due to their intrinsically low permeability. Carbonate-cemented sediments are predominantly in the montmorillonite-kaolinite and illite-chlorite zones in which dolomite is replaced by calcite with increased tempeature. The carbonate cement occurs in a range of grain sizes and textures, from microcrystalline to coarser grained poikiloblasts.

Inception of the calc-silicate zone marks a pronounced change in the nature of the cementation. The earlier-formed carbonate cement is gradually replaced by wairakite and epidote. These minerals nucleate and grow almost exclusively within the carbonate cement, and rarely replace the framework grains. In sandstone samples from the highest temperature parts of the calc-aluminum silicate zone, grain boundaries between pore-filling calc-silicates and detrital framework grains may approach a planar configuration.

The temperature/depth dependent nature of mineral zonation in the Cerro Prieto geothermal field has been identified in petrologic studies of approximately 50 wells. Mineralogic isograds for wairakite, epidote, and prehnite shown in two representative cross-sections (B and D, Fig. 13) closely parallel the measured (or isotopically calculated) isotherms (A and C, Fig. 13). Although both fluid and bulk rock compositions may vary throughout the systems, there is an overall systematic correlation between the spatial distribution of isotherms and the calc-silicate isograds in the Cerro Prieto geothermal system. Mineral distributions in shales are similar to those reported for sandstone. The mineralogic isograds in the shales invariably occur at systematically greater depth/temperature than in the interbedded sandstones. This observation

is consistent with a lower permeability and more limited mass transfer in shale horizons. Discussions of calc-silicate minerals presented below are restricted to occurrences in sandstone and siltstone.

Calc-silicate minerals include wairakite, epidote, prehnite, actinolite, calcium clinopyroxene and sphene. These minerals occur as coarser grained pore-fillings (e.g., wairakite, epidote, prehnite, and clinopyroxene), finer grained authigenic matrix (e.g., actinolite, sphene, clinopyroxene), and within veins that are occasionally monomineralic (i.e., all except sphene). Representative compositions of coexisting calc-silicate mineral assemblages are given in Table 2.

•Wairakite has been identified in samples from 40 of 53 geothermal wells from the Cerro Prieto field. Wairakite first appears as a pore-filling cement in samples believed to have reacted with geothermal fluids at temperatures of 200° to 230°C. Petrographically, sandstones which contain abundant wairakite cement have a distinctive "dark" appearance when viewed under cross-polarized light, even if individual crystals are not discernable. Rare, coarse-grained (<0.05 mm in max. diameter) wairakites are subidioblastic and exhibit characteristic lamellar twinning parallel to crystal faces. When present, these coarse-grained wairakites typically form in equigranular mosaic aggregates; wairakite forms almost exclusively as pore-filling cement and only rarely has it been observed as a replacement of detrital feldspars or lithic clasts.

Compositionally, wairakite is close to being stoichiometric $Ca_2Al_2Si_4O_{12}\cdot 2H_2O$. The results of 16 microprobe analyses (Figure 14a) indicate that molar Ca/Na+K+Ca ranges from 0.90 to 1.00 with a mean of 0.97±.03. K_2O is not present in appreciable quantities (<0.03 wt%) although these wairakites coexist with highly potassic, authigenic microcline. The limited analcime content of these wairakites may reflect their formation through the replacement of earlier-formed calcite, as is also suggested by the invariably close spatial

relationship between these phases if both are present. At higher temperatures (near 300°C) wairakite is replaced by epidote or prehnite.

•Epidote is the most abundant calc-silicate in the Cerro Prieto geothermal field. It has been petrographically identified in 40 of 53 studied wells where it occurs as veins and interstitial cement within sandstones and shales at temperatures >230°C. Radiating aggregates of fine-grained acicular crystals within carbonate pore-filling cement typify epidotes at temperatures slightly >230°C. These crystals appear to have nucleated along grain boundaries of detrital quartz or fine-grained (oxide?) inclusions within the carbonate cement. In the latter case the low-temperature epidotes are commonly intergrown with fine-grained granular sphene. At greater depths and temperatures (>300°C) epidotes are considerably coarser grained (<0.5 mm in max. dimension) and more prismatic, and show evidence of replacement of calcite or wairakite. Interstitial epidote crystals are typically molded about and partially embaying the sub-rounded edges of detrital framework grains. Away from the boundaries of framework grains, epidotes become subidioblastic and densely intergrown. In a given sandstone/siltstone, epidote never exceeds the grain size of detrital framework constituents. They are rarely porphyroblastic and never poikiloblastic.

Compositionally, epidotes from the Cerro Prieto geothermal field exhibit a substantial range in solid solution. Analysis of over 400 epidotes plotted on a compositional frequency histogram (Figure 15a) yield a normal distribution for pistacite (Ps) contents between 11 to 31. Compositional zoning within individual crystals or between crystals from the same cutting chip (always separated by less than 5 mm) is generally less than 5 mole % Ps. Epidotes from different drill cuttings representative of the same depth interval of a given well, do show significant compositional variations (Figure 16), perhaps indicating that compositional homogeneity is areally restricted (even to a centimeter scale).

In general, compositional zoning in the Cerro Prieto epidotes is much less than that observed in epidote minerals from the Salton Sea geothermal system.

Although there is considerable variation in the composition of geothermal epidotes, several interesting systematic relations are apparent between the averaged values of $X_{Ca_2Fe_3Si_3O_{12}(OH)}$ and depth, temperature and coexisting mineral assemblages (Fig. 16). In the calcite-wairakite mineral zones X_{ps} is usually <20 and either decreases or remains constant with increasing depth until the prehnite isograd is reached. X_{ps} in epidote coexisting with prehnite increases with increasing depth and temperatures to values slightly >20. The most iron-rich epidotes occur at horizons that closely correspond to the first appearance of geothermal biotite. With increasing depth and temperature below the biotite isograd X_{ps} in epidote decreases. Similar compositional trends of the more iron-rich epidotes from the Salton Sea geothermal system are found within the biotite zone (McDowell and Elders, in preparation).

•Prehnite is a common phase in veins and an intergranular mineral in sandstones at $\gtrsim$300°C. Prehnite can comprise up to 20% of the mode of sandstone samples, but more commonly <5%. It has been petrographically identified in cuttings from 26 of 53 studied wells. In sandstone cuttings it invariably occurs as coarse-grained (up to 2 mm, but generally less than 1 mm, in max. dimension) xenoblastic poikiloblasts enclosing detrital framework grains, and to a lesser extent, other pore-filling calc-silicates. These poikiloblasts typically exhibit characteristic "bow tie" extinction.

Prehnite compositions show a wide range in $Fe/Fe+Al^{VI}$. A histogram of 101 prehnite analyses (Figure 15b) indicates that $Fe/Fe+Al^{VI}$ ranges from 0.01-0.28 mole %, although the majority of the prehnites plot at <0.125 mole %. Compositional variations within individual prehnite poikiloblasts are large (e.g., $Fe/Fe+Al^{VI}$ for a vein prehnite in well M48 at 1199 m ranges from .059 to .279 with oscillatory zoning, whereas included and co-existing epidotes vary

only from Ps 20 to 25). These large compositional variations in prehnites as well as their typically coarse grain size may be a reflection of relatively high growth rates (in comparison to epidote, for example) which could have allowed development of kinemetrically controlled compositional gradients adjacent to the crystal/fluid interface during growth.

Average prehnite compositions in individual wells do not exhibit systematic variations as a function of depth. Prehnites in well M84 exhibit some Fe-enrichment (as do co-existing epidotes), whereas prehnites in well T366 and M125 show little variation in Fe-content with depth (Figure 16). In low grade, fossil metamorphic terrains, prehnites exhibit patterns of both increased (Surdam, 1973; Kunioshi and Liou, 1976) and decreased (Evarts and Schiffman, 1983) Fe-content as a function of increased stratigraphic-depth.

•Actinolite has been identified in cuttings from relatively few wells - approximately 10 of the 53 wells studied - and always in samples believed to have reacted with fluids at temperatures between 300° and 350°C. Authigenic amphiboles typically occur in coarse (0.5 mm), brown-tinted, feathery masses. These masses exhibit pervasive, closely spaced, parallel striations which may be crypto-crystalline fibers which have coalesced to form the larger optically homogeneous domains. Such coarse-grained amphiboles, which comprise <1% of the total mode of a given sandstone sample, appear to form through the recrystallization of detrital framework grains and through the replacement of pre-existing pore-filling material such as calcite or detrital/authigenic phyllosilicate matrix.

Virtually all sandstone cuttings from the calc-silicate zone contain some (secondary) pore space which is variably filled with mattes of randomly-oriented, very fine-grained, acicular crystallites. The optical properties of these crystallites (pale green to colorless, moderate (+) relief, and near parallel extinction) are compatible with either actinolite or chlorite, perhaps

both. Rarely, these crystallites appear to grade perceptively into the coarser, brownish actinolitic aggregates described above.

Compositionally, the 17 hydrothermal amphiboles which have been analyzed (Figure 17) are all actinolite, according to the I.M.A. classification scheme (Leake, 1978), with molar Mg/Mg+Fe+Mn ranging from 0.62 to 0.82. These compositions partially, but not completely, overlap the measured Mg/Mg+Fe+Mn ratios of amphiboles from other active geothermal systems (Figure 4). Compositional zoning within individual aggregates of Cerro Prieto actinolites has not been observed.

All of the Cerro Prieto actinolites contain very low Al^{IV} (<0.20 Al^{IV}/15 cations) and low M4 Na (<0.10/15 cations). These actinolites (as well as those from other active geothermal fields described earlier) are compositionally similar to greenschist facies amphiboles from low P_{H_2O}, high fluid/rock, fossil hydrothermal systems such as ophiolites (Evarts and Schiffman, 1983).

•Pyroxene has been identified in samples from 9 of 53 studied wells at temperatures between 300° and 350°C. These pyroxenes typically occur as subidioblastic prisms (<0.2 mm in max. dimension) with well-developed (110) form crystal faces and cleavage. These prismatic pyroxenes typically terminate into acicular projections elongate parallel to (110). Pyroxenes occur exclusively as pore-filling cement or in veins. The pore-filling varieties often occur as fine-grained aggregates, spherulitic in part. These hydrothermal pyroxenes are usually colorless; however, greenish, slightly pleochroic clinopyroxene occurs in sandstone which contains microcline and abundant sphene.

The results of 66 electron microprobe analyses (Figure 18) indicate that the Cerro Prieto pyroxenes are all highly calcic augite, with M2 sites filled in excess of 90% by Ca. Molar Mg/Mg+Fe+Mn range from 0.23 to 0.90. Green

clinopyroxenes in well T366 at 2850 m are in part the most hedenbergitic pyroxenes in the Cerro Prieto field. Colorless pyroxenes analyzed from separate cuttings at the same depth interval are the most diopsidic.

In all the wells in which pyroxenes were analyzed in drill cuttings from more than one depth interval (i.e., M93, M125, and T366), colorless clinopyroxenes show an increase in Mg/Mg+Fe with depth (e.g., in well T366 from ~0.60 at 2655 m to a maximum of 0.90 at 2985 m). Mg-enrichment in pyroxene and sympathetic Fe-enrichment in co-existing epidotes as a function of increased depth in well T366 may be related to increased f_{O_2} in the fluid phase.

• Sphene is a ubiquitous mineral in samples representative of a large depth and temperature interval in virtually all of the wells studied. Authigenic sphene has been identified in samples from the chlorite-illite zone, so it probably has crystallized at temperatures as low as 150°C. Typically, sphene forms in very fine-grained xenoblastic aggregates within pore-filling cement, often spatially associated with detrital(?) opaque minerals which may serve as sources of Ti. In calc-silicate zone samples, sphenes are generally coarser (<0.10 mm) and may exhibit subidioblastic, wedge-shaped prismatic forms. Microprobe analyses of sphenes from a few different depth intervals in well M53 indicate that these compositions are fairly homogeneous and close to $Ca_{1.00}(Al_{0.36}Ti_{0.61}Mg_{0.03})Si_{1.00}O_{4.00}(F,OH)_{0.36}O_{0.61}$.

• Other Authigenic Silicate Minerals include (in order of decreasing modal abundance): quartz, microcline, biotite, chlorite, and sericite.

Quartz typically accounts for 40-60% of sandstone modes in the calc-silicate zone, mostly in the form of recrystallized detrital framework grains which may or may not develop planar interfaces with calc-silicate minerals. Quartz also occurs as pore-filling cement, but quartz-cemented sandstones are significantly subordinate to calc-silicate cemented sandstones at $\gtrsim$300°C.

Microcline, typically exhibiting well-developed cross-hatched twinning, accounts for 5-10% of sandstone modes in calc-silicate zone mineral assemblages. These feldspars apparently formed by recrystallization of detrital plagioclase and alkali feldspar framework grains. The results of 33 analyses (Figure 14b) indicate that compositionally, the microclines range from Or 91-97 with a mean near Or 95. No authigenic plagioclase feldspars have been petrographically identified in samples from the Cerro Prieto geothermal field although "plagioclase" typically comprises between 0-10% of the sandstone mineral mode in quantitative XRD analysis (Johnson, 1978) in samples from all depths.

Biotite is a minor phase (<5% of the mode) in some sandstone cuttings from the higher temperature (i.e., 300°-350°C) portion of the calc-silicate zone where it occurs as fine-grained aggregates within the sandstone matrix and as coarser pseudomorphs of detrital phyllosilicates. Compositionally, the geothermal biotites are characterized by low Al^{VI} (<0.23 Al^{VI}/formula unit), low interlayer site occupancy (typically <0.80 Na+K/formula unit), and by molar Mg/Mg+Fe+Mn ratios which vary between 0.58 and 0.87 (Figure 17). Systematic compositional variations in biotite as a function of depth, such as been reported in the Salton Sea geothermal field (McDowell and Elders, 1980), were not observed.

Chlorite and sericite are minor matrix phases in the lower temperature (i.e., 230°-300°C) portion of the calc-silicate zone. These minerals, whose presence is largely determined by X-ray techniques, are invariably fine-grained and difficult to differentiate petrographically from fine-grained actinolite. Microprobe analyses of a few chlorites in well M53 indicate that they are ripidolites and pycnochlorites (Hey, 1954).

Phase Relations Among Calc-Silicates and Geothermal Reservoir Fluids

Thermodynamic properties of chemical reactions that depict observed calc-silicate phase relations in the Cerro Prieto geothermal system allows

critical evaluation of the extent to which temperature, pressure and mineral compositions effect the activities and fugacities of aqueous and gaseous species in geothermal reservoir fluids. Phase diagrams depicting equilibrium constraints among geothermal reservoir fluids and epidote-prehnite and epidote-pyroxene solid solutions from wells M84 and T366 are shown in Figures 19 and 20, respectively. The symbols in these diagrams correspond to the values of $a_{Ca^{++}}/a^2_{H^+}$ and $a_{Fe^{+++}}/a^3_{H^+}$ compatible with observed compositions of epidote and prehnite solid solutions and of the range of $a_{Ca^{++}}/a^2_{H^+}$ and $a_{Mg^{++}}/a^2_{H^+}$ consistent with coexisting epidote and calcium clinopyroxenes (Table 2). For the latter assemblage the range in cation activity ratios corresponds to fluids in equilibrium with epidote and pyroxene solids solutions in the presence of either prehnite solid solution in accord with the reactions

$$1.5\ Ca_2Al(AlSi_3O_{10})(OH)_2 + 2H^+ \rightleftarrows Ca_2Al_3Si_3O_{12}(OH) + Ca^{++} + 1.5\ SiO_2 + 2\ H_2O \qquad (8)$$

and

$$Ca_2Al_3Si_3O_{12}(OH) + CaMgSi_2O_6 + 2H^+ \rightleftarrows 1.5\ Ca_2Al(AlSi_3O_{10})(OH)_2 + 0.5\ SiO_2 + Mg^{++}, \qquad (9)$$

or for the coexistence with tremolite solid solutions in accord with the reactions

$$5\ CaMgSi_2O_6 + 6H^+ + \rightleftarrows Ca_2Mg_5Si_8O_{22}(OH) + 3\ Ca^{++} + 2\ SiO_2 + 2\ H_2O \qquad (10)$$

and

$$Ca_2Mg_5Si_8O_{22}(OH)_2 + 6H^+ \rightleftarrows 2\ CaMgSi_2O_6 + 3\ Mg^{++} + 4\ SiO_2 + 4\ H_2O\ . \qquad (11)$$

For a given temperature, pressure and coexisting epidote and pyroxene compositions the prehnite limiting reactions represent the maximum $a_{Ca^{++}}/a^2_{H^+}$ (reaction 8) and the minimum $a_{Mg^{++}}/a^2_{H^+}$ (reaction 9) and consequently the maximum $a_{Ca^{++}}/a_{Mg^{++}}$ ratios in the coexisting geothermal fluids. In contrast it can be seen in Figure 20 that the tremolite limiting reactions (10 and 11) denote the minimum value of $a_{Ca^{++}}/a_{Mg^{++}}$.

Calculated values of $a_{Ca^{++}}/a^2_{H^+}$ in geothermal fluids coexisting with epidote and either prehnite or pyroxene solid solutions are shown as a function of depth within four geothermal wells in Figure 21. In addition, the assemblage of biotite-K-feldspar-calcium clinopyroxene from 2240 m in well M125 as represented by the reaction

$$3\ CaMgSi_2O_6 + K\ AlSi_3O_8 \rightleftharpoons K\ Mg_3(AlSi_3O_{10})(OH)_2 + 6H^+ + 3\ Ca^{++} + 6\ SiO_2 + 2\ H_2O \qquad (12)$$

is given in Figure 21b (hexagon). The values of log $a_{Ca^{++}}/a^2_{H^+}$ in geothermal fluids compatible with these three types of calc-silicate assemblages are within the range of ~6.5 to 7.5 at depths between 1.4 and 3.0 km. Note that the calculated cation activity ratios for alternate mineral assemblages at similar depths are in close agreement as shown for wells M125 and M84.

Dependence on $a_{Ca^{++}}/a_{Mg^{++}}$ in geothermal fluids coexisting with epidote and calcium clinopyroxene solid solutions as a function of temperature and epidote composition are given in Figure 22. Although there is considerable scatter in these data it appears that $a_{Ca^{++}}/a_{Mg^{++}}$ increases with increasing temperature and $X_{Ca_2Fe_3Si_3O_{12}(OH)}$. This is most certainly true for the prehnite limiting assemblages based on reactions (8) and (9). Solid symbols in Figure 22a represent geothermal reservoir fluids from Cerro Prieto reported by Fausto et al. (1979) where we have made the provisional approximation that

$\gamma_{Ca^{++}}/\gamma_{Mg^{++}} \sim 1$. Note that the general trends of the calculated and measured Ca++ to Mg++ ratios are in close agreement. At ~310°C fluids appear to be compatible with the prehnite limiting reactions (8) and (9), but at $\gtrsim$310°C fluids are closer to the tremolite limiting reactions (10) and (11).

Note in Figure 22a that the calculated $a_{Ca^{++}}/a_{Mg^{++}}$ ratio in the fluid phase coexisting with the observed assemblage of epidote-prehnite-clinopyroxene for well M84 (Table 2, 1557 m) is ~1.5 log units larger than the measured fluid compositions reported by Fausto et al. (1979). The measured composition of the fluid appears to be closer to the calculated trend of $a_{Ca^{++}}/a_{Mg^{++}}$ compatible with tremolite-epidote-clinopyroxene assemblages. It is possible that the fluids produced from well M84 are originating from fracture systems or permeable sandstone aquifers where tremolite bearing assemblages are stable, and that these fluids are not in equlibrium with prehnite assemblages observed in the drill cuttings.

The $a_{Ca^{++}}/a_{Mg^{++}}$ calculated from epidote-pyroxene assemblages using tremolite-limiting reactions in the Cerro Prieto geothermal system are consistent with the same activity ratio calculated from biotite-tremolite-epidote assemblages from the Salton Sea geothermal system (Bird and Norton, 1981: ~10^3 to $10^{3.5}$ at $\gtrsim$330°C). Calculations in both systems suggest a smooth increase in $a_{Ca^{++}}/a_{Mg^{++}}$ with increasing temperature. However, $a_{Ca^{++}}/a_{Mg^{++}}$ calculated for epidote-pyroxene-prehnite assemblages (Fig. 20) is about an order of magnitude larger than values calculated from either geothermal system for tremolite-bearing assemblages.

Fugacities of $O_2(g)$ compatible with the epidote and pyroxene assemblages of Figure 21 are shown in Figure 23 as a function of temperature and $X_{Ca_2Fe_3Si_3O_{12}(OH)}$. The symbols denote Log f_{O_2} in accord with reactions (8) or (10) and

$$12\ Ca_2FeAl_2(Si_3O_{12})(OH) \rightleftarrows 8\ Ca_2Al_3Si_3O_{12}(OH) + 4\ Ca^{++} + 12\ SiO_2 + 12\ CaFeSi_2O_6 + 8H^+ + 3\ O_2(gas) + 2\ H_2O \quad (15)$$

The calculated oxygen fugacities increase with increasing temperature and with $X_{Ca_2Fe_3Si_3O_{12}(OH)}$ in epidote-bearing mineral assemblages. The calculated $f_{O_2(gas)}$ is about five orders of magnitude larger in the Salton Sea relative to the Cerro Prieto system (Fig. 23B). This contrast is consistent with the presence of trace amounts of hematite in the Salton Sea system, and a lack of hematite in the Cerro Prieto system. The more reducing conditions for Cerro Prieto are also consistent with the occurrence of prehnite in the calc-silicate assemblages from this system and its absence in the more oxidizing environment of the Salton Sea geothermal system (see phase diagrams in Bird and Helgeson, 1981, Fig. 12A; Cavarretta et al., 1982, Fig. 7).

Concluding Remarks

Calcium silicates in the system $CaO-MgO-FeO-Fe_2O_3-Al_2O_3-TiO_2-SiO_2-H_2O$ are an important group of rock forming minerals in worldwide geothermal areas. Deep drilling in these active hydrothermal systems has shown that there is a systematic zoning of metasomatic calc-silicates with depth. This zoning pattern is found in geothermal systems with a wide variety of host rock compositions (Table 1) and represents the progressive dehydration of both structural and zeolitic water from calc-silicate minerals with increasing temperature (Figures 5 and 6). Few geothermal calc-silicates correspond to compositions of their stoichiometric analogs, but their compositional characteristics are well known for only a few of the worldwide geothermal areas. An important aspect of these minerals that has largely been overlooked is a detailed analysis of their light stable isotopic compositions, their structural states, the extent to which substitutional ordering occurs among cations on energetically distinct sites,

and the stoichiometry of zeolitic water in the Ca-zeolites. These properties are critical to a complete understanding of calc-silicate mineralization in active geothermal systems.

Although the zoning of calc-silicates with depth can be readily correlated with measured temperatures (Figure 6), there are only subtle systematic variations in the compositional characteristics of these minerals with respect to the measured parameters of depth, temperature, pressure, and mineralogic phase relations. It appears that the observed compositional trends are dependent to a large extent on the composition of the host rocks and the geothermal fluids, and the time rate of change of these parameters together with that of temperature, pressure, and fluid flow during the thermal evolution of a geothermal system.

Thermodynamic analysis of the compositional relations of mineral assemblages that include calc-silicates commonly leads to a close correlation among predicted and observed geothermal fluid compositions (Bird and Helgeson, 1981; Bird and Norton, 1981; Giggenbach, 1981; Capuano and Cole, 1982). However, it is apparent from the compositions of coexisting calc-silicates presented above that certain mineral pairs, such as epidote-garnet and pyroxene-actinolite, may not represent an equilibrium partitioning of octahedral cations among these minerals. It is highly likely that many of the observed mineral assemblages in active geothermal systems do not represent equilibrium at the temperatures, pressures and fluid compositions measured in deep drill holes. Calculations presented by Bird and Norton (1981), Capuano and Cole (1982), and Cavarretta (1982) clearly show that metastable phases and partial equilibrium exist at temperatures $\lesssim$300°C in some geothermal systems.

Mineral assemblages and zoning patterns found in the upper three kilometers of the earth's crust in areas of active geothermal activity are similar to phase relations reported in low pressure regional and contact metamorphic rocks. The

advantage of investigating calc-silicates in active geothermal systems relative to their paleo-metamorphic analogs is that temperatures, pressures, and fluid compositions associated with observed mineral assemblages can be measured in deep drill holes. This allows for critical evaluation of both quantitative and qualitative techniques for predicting the intensive thermodynamic variables associated with the formation of calc-silicate minerals assemblages.

ACKNOWLEDGEMENTS

The research described above was supported by the U.S. Department of Energy contract no. DE-FC07-80ID12145. We thank our colleagues at UCR, Lawrence Berkeley Laboratory, and La Comisión Federal de Electricidad for their assistance and cooperation during our studies at Cerro Prieto. Special thanks are due to Denis Norton for the use of computer facilities at the University of Arizona.

REFERENCES

Barager, K. E. and Beeson, M. H., 1981, Hydrothermal alteration in research drill hole Y-2, Lower Geyser Basin, Yellowstone National Park, Wyoming: Am. Mineral., v. 66, p. 473-490.

Bence, A. E. and Aldee, A. L., 1968, Empirical correction factors for the electron microanalysis of silicates and oxides: Jour. Geol., v. 76, p. 382-406.

Bermejo, F. J., Navarro, F. X., Castillo, B., Esquer, C. A. and Cortez, A., 1979, Pressure variation at the Cerro Prieto reservoir during production: in Proceedings of the Second Symposium on the Cerro Prieto Geothermal Field, Oct. 1979, Mexicali, v. 2, p. 473-497.

Bird, D. K. and Norton, D. L., 1981, Theoretical predictions of phase relations among aqueous solutions and minerals: Salton Sea geothermal system: Geochim. Cosmochim. Acta, v. 45, p. 1479-1493.

Bird, D. K. and Helgeson, H. C., 1980, Chemical interaction of aqueous solutions with epidote-feldspar mineral assemblages in geologic systems. I. Thermodynamic analysis of phase relations in the system CaO-FeO-Fe_2O_3-SiO_2-H_2O-CO_2: Am. Jour. Sci., v. 280, p. 907-941.

Bird, D. K. and Helgeson, H. C., 1981, Chemical interaction of aqueous solutions with epidote-feldspar mineral assemblages in geologic systems. II. Equilibrium constraints in metamorphic/geothermal processes: Am. Jour. Sci., v. 281, p. 576-614.

Browne, P. R. L., 1978, Hydrothermal alteration in active geothermal fields: Ann. Rev. Earth Planet. Sci., v. 6, p. 229-250.

Browne, P. R. L., 1977, Occurrence of hydrothermal alteration of diabase, Heber geothermal field, Imperial Valley, California: Preliminary report: University of California, Riverside/Institute of Geophysics and Planetary Physics report 77/9, 61 p.

Browne, P. R. L. and Ellis, A. J., 1970, The Ohaki-Broadlands hydrothermal area, New Zealand: Mineralogy and related geochemistry: Am. Jour. Sci., v. 269, p. 97-131.

Capuano, R. and Cole, D. R., 1982, Fluid mineral equilibria in a hydrothermal system, Roosevelt Hot Springs, Utah: Geochem. Cosmochim. Acta, v. 46, p. 1353-1364.

Cavarretta, G., Gianelli, G. and Puxeddu, M., 1982, Formation of authigenic minerals and their use as indicators of the chemicophysical parameters of the fluid in the Larderello-Travale geothermal field: Econ. Geol., v. 77, p. 1071-1084.

Cavarretta, G., Gianelli, G. and Puxeddu, M., 1980, Hydrothermal metamorphism in the Larderello geothermal field: Geothermics, v. 9, p. 297-314.

Coombs, D. S., Kawachi, Y., Houghton, B. F., Hyden, G., Pringle, I. J. and Williams, J. G., 1977, Andradite and andradite-grossular solid solutions in southern New Zealand: Contr. Min. Pet., v. 63, p. 229-246.

Einaudi, M. T., Meinert, L. D. and Newberry, R. J., 1981, Skarn deposits: Econ. Geol., 75th Anniv. Volume, p. 317-391.

Elders, W. A., 1979, The geological background of the geothermal fields of the Salton Trough: in Geology and Geothermics of the Salton Trough (Elders, W. A., ed.), Guidebook prepared for the Geological Society of America 92nd Annual Meeting, Nov. 1979, San Diego, 19 p.

Elders, W. A., Hoagland, J. R. and Williams, A. E., 1981, Distribution of hydrothermal mineral zones in the Cerro Prieto geothermal field of Baja California, Mexico: Geothermics, v. 10, p. 245-253.

Elders, W. A., Hoagland, J. R., McDowell, S. D. and Cobo, J. M., 1979, Hydrothermal mineral zones in the geothermal reservoir of Cerro Prieto: Geothermics, v. 8, p. 201-209.

Ellis, A. J. and Mahon, W. A. J., 1977, Chemistry and Geothermal Systems, Academic Press, 392 pp.

Evarts, R. C. and Schiffman, P., 1983, Submarine hydrothermal metamorphism of the Del Puerto ophiolite, California: Am. Jour. Sci., v. 283, pp. 289-340.

Fausto, J. J., Sánchez, A., Jiménez, M. E., Esquer, I. and Ulloa, F., 1979, Hydrothermal geochemistry of the Cerro Prieto geothermal field: in Proceedings of the Second Symposium on the Cerro Prieto Geothermal Field, Oct. 1979, Mexicali, v. 2, p. 199-223.

Ferrer, H., 1983, Hydrothermal petrology and isotopic geochemistry of the Tongonan geothermal field, Philippines: University of California, Riverside, unpublished M.S. thesis.

Fuis, G. S., Mooney, W. D., Healy, J. H., McMechan, G. A. and Lutter, W. J., 1982, Crustal structure of the Imperial Valley region: U.S. Geological Survey Prof. Paper 1254, "The Imperial Valley Earthquake of October 15, 1979", p. 25-50.

Ghose, S. and Ganguly, J., 1982, Mg-Fe Order-disorder in Ferromagnesian Silicates: in Advances in Physical Chemistry, (Saxena, S. K., ed.) Springer-Verlag, v. 2, p. 3-99.

Giggenbach, W. F., 1981, Geothermal mineral equilibria: Geochem. et Cosmo. Acta, v. 45, p. 393-410.

Hammerstrom, L. T. and Brown, T. H., 1983, Internally consistent thermodynamic data and phase relations in the $CaO-Al_2O_3-SiO_2-H_2O$ system: Contrib. Min. and Petrol. (in press).

Hayashi, M. and Yamasaki, T., 1976, Hydrothermal alteration of pyroxene andesites in the Otake geothermal area, Japan: in Proceedings, International Symposium on Water-Rock Interaction (Cadek, J. and Paces, T., eds.), Prague, 1979, Geological Survey of Czechoslovakia, p. 158-169.

Helgeson, H. C., 1967, in Researches in Geochemistry, v. 2 (Abelson, P. H., ed.), New York, Wiley & Sons, p. 362-404.

Helgeson, H. C., Kirkham, D. H. and Flowers, G. C., 1982, Theoretical prediction of the thermodynamic behavior of aqueous electrolytes at high pressures and temperatures. IV. Calculation of activity coefficients, osmotic coefficients, and apparently molal and standard and relative partial molal properties to 5 kb and 600°C: Am. Jour. Sci.

Helgeson, H. C. and Aagaard, P., 1983, Activity/composition relations among silicates and aqueous solutions. I. Thermodynamics of intrasite mixing and substitutional order/disorder in minerals: Am. Jour. Sci., v. 283.

Helgeson, H. C., Delany, J. M., Nesbitt, H. W. and Bird, D. K., 1978, Summary and critique of the thermodynamic properties of rock-forming minerals: Am. Jour. Sci., v. 278-A, 229 p.

Helgeson, H. C. and Kirkham, D. H., 1974a, Theoretical prediction of the thermodynamic behavior of aqueous electrolytes at high pressures and temperatures. I. Summary of the thermodynamic/electrostatic properties of the solvent: Am. Jour. Sci., v. 274, p. 1089-1198.

Helgeson, H. C. and Kirkham, D. H., 1974b, Theoretical prediction of the thermodynamic behavior of aqueous electrolytes at high pressures and temperatures. II. Debye-Huckel parameters for activity coefficients and relative partial mold properties: Am. Jour. Sci., v. 274, p. 1199-1261.

Helgeson, H. C. and Kirkham, D. H., 1976, Theoretical prediction of the thermodynamic behavior of aqueous electrolytes at high pressures and temperatures. III. Equation of state for aqueous species at infinite dilution: Am. Jour. Sci., v. 276, p. 97-240.

Hey, M. H., 1954, A new review of the chlorites: Mineralog. Mag., v. 30, p. 277-292.

Holdaway, M. J., 1972, Thermal stability of aluminum-iron epidote as a function of f_{O_2} and iron content: Contr. Min. Pet., v. 36, p. 307-340.

Johnson, P. D., 1978, Use of automated X-ray diffraction analysis in studies of natural hydrothermal systems: in Advances in X-ray Analysis, New York, Plenum Press, v. 21, p. 267-274.

Keith, T. E. C., Muffler, L. P. J. and Cramer, M., 1968, Hydrothermal epidote formed in the Salton Sea geothermal system, California: Am. Mineral., v. 53, p. 1635-1644.

Kendall, C., 1976, Petrology and stable isotope geochemistry of three wells in the Buttes area of the Salton Sea geothermal field, Imperial Valley, California, U.S.A.: University of California, Riverside/Institute of Geophysics and Planetary Physics report 76/17, 227 p., M.S. thesis.

Kitamura, K., 1975, Al-Fe partitioning between garnet and epidote from the contact metasomatic copper deposits of the Chichiku Mine, Japan: Econ. Geol., v. 70, p. 725-738.

Kristmannsdottir, H., 1981, Wollastonite from hydrothermally altered basaltic rocks in Iceland: Mineralog. Mag., v. 44, p. 95-99.

Kristmannsdottir, H. and Tomasson, J., 1978, Zeolite zones in geothermal areas in Iceland: in Natural Zeolites (San, L. B. and Mumpton, F. A., eds.), Oxford, Pergamon Press, p. 277-284.

Kristmannsdottir, H. and Tomasson, J., 1976, Nesjavellir-hydrothermal alteration in a high-temperature area: in Proceedings, International Symposium on Water-Rock Interaction (Cadek, J. and Paces, T., eds.), Prague, 1974, Geological Survey of Czechoslovakia, p. 170-177.

Kuniyoshi, S. and Liou, J. G., 1976, Burial metamorphism of the Karmutsen volcanic rocks, northeastern Vancouver Island, British Columbia: Am. Jour. Sci., v. 276, p. 1096-1119.

Kwak, T. A. P., 1978, Conditions of formation of the King Island scheelite contact skarn, King Island, Tasmania, Austria: Am. Jour. Sci., v. 278, p. 969-999.

Lan, C. Y., Liou, J. G. and Seki, Y., 1980, Investigations of drillhole core sampled from Tatum geothermal area, Taiwan: in Proceedings of the Third International Symposium on Water-Rock Interactions, Edmonton, 1980, p. 183-185.

Liou, J. G., 1973, Synthesis and stability relations of epidote, $Ca_2Al_2FeSi_3O_{12}(OH)$: Jour. Petrology, v. 14, p. 381-413.

Lockner, D. A., Summers, R., Moore, D. and Byerlee, J. D., 1982, Laboratory measurements of reservoir rocks from The Geysers geothermal field, California: International Jour. Rock Mech., Min. Sci., Geomech. Abstracts, v. 19, p. 65-80.

McCallister, R. H., Finger, L. W. and Ohashi, Y., 1976, Intracrystalline Fe^{++}-Mg equilibric in three natural Ca-rich clinopyroxenes: Am. Mineral., v. 61, p. 671-676.

McDowell, S. D. and Elders, W. A., 1980, Authigenic layer silicate minerals in borehole Elmore 1, Salton Sea geothermal field, California, U.S.A.: Contr. Mineral. Petrol., v. 74, p. 293-310.

McDowell, S. D. and Elders, W. A., in preparation, Active metamorphism in the Salton Sea geothermal field: (I) Metamorphic mineralogy and mineral chemistry in borehole Elmore 1.

McDowell, D. and McCurry, M., 1977, Active metamorphism in the Salton Sea geothermal field, California: Mineralogical and mineral changes with depth and temperature in sandstone: Geol. Soc. America Abstr. with Prog., v. 9, p. 1088.

McDowell, D. and McCurry, M., 1978, Mineralogical variations in borehole Elmore #1, Salton Sea geothermal area: Preliminary report: University of California, Riverside/Institute of Geophysics and Planetary Physics report 78/11, 37 p.

Miyashiro, A. and Seki, Y., 1958, Enlargement of the composition field of epidote and piemontite with rising temperature: Am. Jour. Sci., v. 256, p. 423-430.

Morgan, B. A., 1975, Mineralogy and origin of skarns in the Mount Morrison Pendant, Sierra Nevada, California: Am. Jour. Sci., v. 275, p. 119-142.

Mueller, R. F., 1961, Analysis of relations among Mg, Fe and Mn in certain metamorphic minerals: Geochem. Cosmochim. Acta, v. 25, p. 267-296.

Muffler, L. P. J. and Doe, B., 1968, Composition and mean age of detritus of the Colorado River in the Salton Trough, southeastern Californa: J. Sediment Petrol., v. 38, p. 384-399.

Muffler, L. P. J. and White, D. E., 1969, Active metamorphism of Upper Cenozoic sediments in the Salton Sea geothermal field and the Salton Trough, southeastern California: Geol. Soc. America Bull., v. 80, p. 157-182.

Naboko, S. I., 1970, Facies of hydrothermally altered rocks of Kamchatka-Kurile volcanic arc.: Pac. Geol., v. 2, p. 23-27.

Naboko, S. I., 1976, The origin of hydrothermal solutions and related propylitization and argillization in the areas of tectonomagnetic activity: in Proceedings of the International Symposium on Water-Rock Interaction, (Cadek, J. and Paces, T., eds.), Prague, 1974, p. 184-195.

Oki, Y., Hirano, T. and Suzuki, T., 1976, Hydrothermal metamorphism and vein minerals on the Yugawara geothermal area, Japan: in Proceedings of the International Symposium on Water-Rock Interaction, (Cadek, J. and Paces, T., eds.), Prague, 1974, p. 209-222.

Raith, M., 1976, The Al-Fe (III) epidote miscibility gap in a metamorphic profile through the penninic series of the Tauern window, Austria: Contr. Min. Pet., v. 57, p. 99-117.

Reed, M. J., 1976, Geology and hydrothermal metamorphism in the Cerro Prieto geothermal field, Mexico: Proceedings of the Second United Nations

Symposium on the Development and Use of Geothermal Resources, San Francisco, May 1975, v. 1, p. 539-547.

Robinson, P., 1980, The compositional space of terrestrial pyroxenes - internal and external limits: in Reviews in Mineralogy, Pyroxenes (Ribbe, P. H., ed.), v. 7, p. 419-494.

Schiffman, P., 1978, Synthesis and stability relations of pumpellyite: Unpublished Ph.D. dissertation, Stanford University, 191 p.

Seki, Y., 1972, Lower-grade stability limit of epidote in light of natural occurrences: Jour. Geol. Soc. Japan, v. 78, p. 405-413.

Seki, Y., Onuki, H., Okumura, K. and Takashima, I., 1969, Zeolite distribution in the Katayama geothermal area, Onikobe, Japan: Jap. Jour. Geol. Geog., v. 40, p. 63-79.

Sigvaldeson, G. E., 1962, Epidote and related minerals in two geothermal drillholes, Reykjavik and Hveragerdi, Iceland: U.S. Geol. Survey Prof. Paper 450-E, p. 77-79.

Steiner, A., 1977, The Wairakei geothermal area, North Island, New Zealand: Its subsurface geology and hydrothermal rock alteration: New Zealand Geol. Survey Bull., 90, 136 p.

Steiner, A., 1958, Occurrence of wairakite at The Geysers, California: Am. Mineral., v. 43, p. 781.

Sternfeld, J. N., 1981, The hydrothermal petrology and stable isotope geochemistry of two wells in The Geysers geothermal field, Sonoma County, California: University of California, Riverside/Institute of Geophysics and Planetary Physics report 81/7, unpublished M.S. thesis, 215 p.

Strens, R. G. J., 1965, Stability and relations of the Al-Fe epidotes: Mineral. Mag., v. 35, p. 464-475.

Sumi, K., 1965, Hydrothermal rock alteration of the Matsakawa geothermal area, northeast Japan: Geol. Survey Japan Rep., v. 225, 42 p.

Surdam, R. C., 1973, Low-grade metamorphism of tuffaceous rocks in the Karmutsen group, Vancouver Island, British Columbia: Geol. Soc. America Bull., v. 84, p. 1911-1922.

Tewhey, J. D., 1977, Geologic characteristics of a portion of the Salton Sea geothermal field: Lawrence Livermore Laboratory report UCRL-52267, 51 p.

Tomasson, J. and Kristmannsdottir, H., 1976, Investigation of three low-temperature geothermal areas in Reykjavik and its neighbourhood: in Proceedings of the International Symposium on Water-Rock Interaction (Cadek, J. and Paces, T., eds.), Prague, 1974, p. 243-249.

Tomasson, J. and Kristmannsdottir, H., 1972, High temperature alteration minerals and thermal brines, Reykjanes, Iceland: Contr. Mineral. Petrol., v. 36, p. 123-134.

Van de Kamp, P. C., 1973, Holocene continental sedimentation in the Salton Basin, California: A reconnaissance: Geol. Soc. America Bull., v. 84, p. 827-848.

Walther, J. V. and Helgeson, H. C., 1977, Calculation of the thermodynamic properties of aqueous silica and the solubility of quartz and its polymorphs at high pressures and temperatures: Am. Jour. Sci., v. 277, p. 1315-1351.

Yamada, E., 1976, Geological development of the Onikobe caldera and its hydrothermal system: Proceedings of the Second United Nations Symposium on the Development and Use of Geothermal Resources, San Francisco, May 1975, v. 1, p. 665-672.

White, D. E. and Sigvaldeson, G. E., 1962, Epidote in hot-spring systems, and depth of formation of propylitic epidote in epithermal ore deposits: U.S. Geol. Survey Prof. Paper 450-E, p. E80-E84.

FIGURE CAPTIONS

Figure 1. Ternary diagram depicting (in mole percent) stoichiometric compositions of common geothermal minerals in the system CaO-Al_2O_3-Fe_2O_3-FeO-MgO-TiO_2-SiO_2-H_2O.

Figure 2. Ternary diagram (mole percent) depicting measured compositions of Ca-zeolites from active geothermal systems. Heulandite: Yellowstone (Barager and Beeson, 1981); Laumontite: Onikobe (Seki et al., 1969); Otake (Hayashi and Yamasaki, 1976); Wairakei (Steiner, 1977); Wairakite: Otake, Onikobe, Yellowstone, Wairakei, Larderello (Cavarretta et al., 1982); Heber (Browne, 1977).

Figure 3. Measured compositions of geothermal epidote and prehnite solid solutions. $(Fe^{3+}/Fe^{3+}/Al^{VI})x100$ is the mole fraction of octahedral Fe^{3+} in either prehnite ($Ca_2Al(AlSi_3O_{10})(OH)_2$)-Fe-prehnite ($Ca_2Fe(AlSi_3O_{10})(OH)_2$) solid solutions or clinozoisite ($Ca_2Al_3Si_3O_{12}(OH)$)-pistacite ($Ca_2Fe_3Si_3O_{12}(OH)$) solid solutions. Larderello (Cavarretta et al., 1980, 1982), Heber (Browne, 1977), The Geysers (Moore, personal communication), Otake (Hayashi and Yamasaki, 1976), Salton Sea (McDowell and Elders, in preparation).

Figure 4. Ternary diagram depicting (in mole percent) measured compositions of clinopyroxenes, amphiboles, and garnets in active geothermal systems. For references see caption of Fig. 4, and Cavarretta et al. (1982), Elders et al. (1981) and Kendall (1976).

Figure 5. Distribution of calc-silicate mineral assemblages in drillholes from active geothermal systems as a function of depth and temperature.

Figure 6. Measured distribution of calc-silicates as a function of temperature for geothermal systems listed in Table 1.

Figure 7. Phase relations in the system CaO-Al_2O_3-SiO_2-H_2O in the presence of α-quartz (diagram A) and amorphous silica (diagram B), together with an

aqueous phase in which $a_{H_2O} \sim 1$ as a function of the logarithm of $a_{Ca^{++}}/a^2_{H^+}$ in the fluid phase and temperature for pressures corresponding to liquid-vapor equilibrium for H_2O. The long dashed curve represents saturation in the fluid phase with wollastonite, the solid curves denote stability field boundaries for stoichiometric minerals in the system $CaO-Al_2O_3-SiO_2-H_2O$. These diagrams and other phase diagrams and thermodynamic properties of chemical reactions presented elsewhere in this paper are calculated from equations and data reported by Helgeson and others (1978), Helgeson and Kirkham (1974a, 1974b, 1976), Helgeson, Kirkham, and Flowers (1982), and Walther and Helgeson (1977).

Figure 8. Logarithmic activity-activity phase diagrams for the systems $CaO-Al_2O_3-SiO_2-H_2O$ (diagrams A and B), $CaO-K_2O-Al_2O_3-SiO_2-H_2O$ (diagrams C and D, and $CaO-Na_2O-Al_2O_3-SiO_2-H_2O$ (diagrams E and F), at temperatures of 200 and 300°C for pressures corresponding to liquid-vapor equilibrium of H_2O where $a_{H_2O} \sim 1$. Diagrams C through F are for equilibrium in the fluid phase with α-quartz. See figure caption 7 for details. The terms "K-feldspar" and "albite" refer to alkali feldspars in their equilibrium state of order/disorder (see Helgeson et al., 1978).

Figure 9. Logarithmic activity-activity phase diagrams for the system $CaO-MgO-SiO_2-H_2O$ (diagrams A through D) and $CaO-MgO-Al_2O_3-SiO_2-H_2O$ (diagrams E through H) at 200, 250, 300, and 350°C at pressures corresponding to liquid-vapor equilibrium of H_2O where $a_{H_2O} \sim 1$. Diagrams E through H are for equilibrium in the fluid phase with α-quartz. See figure caption 7 for details.

Figure 10. Natural and calculated compositions of coexisting epidote and grandite garnet solid solutions in the system $CaO-Fe_2O_3-Al_2O_3-SiO_2-H_2O$. The symbols represent individual analyses (solid and open symbols) and ranges of mineral compositions (brackets and hatched areas) in active geothermal systems. Broken curve denotes the range of mineral compositions from skarn deposits reported by Morgan (1975) and Kitamura (1975). The solid curves designate com-

positions for various temperatures at 1 kb calculated from equations and data reported by Bird and Helgeson (1980).

Figure 11. Measured compositions of coexisting epidote and prehnite solid solutions from active geothermal systems (solid round symbols), Del Puerto ophiolite (solid square), and basalt host rocks near the Skaergärd intrusion (open hexagons). The solid curve represents the assumed equilibrium partitioning of octahedral Fe^{3+} and Al^{3+} among epidote and prehnite solid solutions which is consistent with an equilibrium constant of $10^{-1.27}$ for reaction (6). See text.

Figure 12. Sketch map of the Cerro Prieto geothermal field, depicting the location of existing wells (open and solid circles), and the trace of the two cross-sections shown in Figure 13.

Figure 13. Cross sections depicting the relationship between isotherms and mineral zones within the Cerro Prieto geothermal field. See Fig. 12 for section locations. Abbreviations: XRD = mineral identified by X-ray diffraction; TS = mineral identified by thin section petrography.

Figure 14. Histograms depicting compositional variations in tectosilicates from the Cerro Prieto geothermal field: (A) wairakite compositions expressed as molar (Ca/Ca+Na+K) x 100; (B) feldspar compositions expressed as mole % orthoclase component.

Figure 15. Histograms depicting molar ($Fe^{+}/Fe^{+}+Al^{VI}$) compositional variations of epidotes (diagram A) and prehnites (diagram B) from the Cerro Prieto geothermal field.

Figure 16. Diagrams depicting the relationship between temperature and depth to the $Fe^{+3}/Fe^{+3}+Al^{VI}$ contents of epidotes (circles) and prehnites (diamonds) in four different wells from the Cerro Prieto geothermal field. Vertical lines connect the compositions of the arithmetic mean (open symbols) of multiple analyses at different depths. Horizontal lines show total

compositional range of all analyses at a given depth; brackets show standard deviation. Abbreviations along the vertical axis of each diagram indicate the depth of first appearance for the minerals. PR = prehnite, PX = clinopyroxene, and BI = biotite. In all of these wells, epidote first appears at a shallower depth than its first reported composition.

Figure 17. Molar Al-Mg-Fe+Mn compositions of hydrothermal biotites and amphiboles from the Cerro Prieto geothermal field. The interior of the diagram is partially contoured in molar Mg/Mg+Mn+Mg.

Figure 18. Ca-Fe-Mg compositions of hydrothermal clinopyroxenes from the Cerro Prieto geothermal field. Wo = wollastonite, En = enstatite, Fs = ferrosilite, Di = diopside, and Hd = hedenbergite.

Figure 19. Theoretical activity-activity phase diagram for the system $CaO-Fe_2O_3-Al_2O_3-SiO_2-H_2O$ at 334° in the presence of quartz and an aqueous phase where $a_{H_2O} \sim 1$ and pressure corresponding to liquid-vapor equilibrium for H_2O. Large broken curves represent saturation in the fluid phase with wollastonite, andradite, or hematite. Thin lines denote constant compositions of epidote, prehnite, and garnet solid solutions. Activity-composition relations for these solid solutions are from equations and data reported by Bird and Helgeson (1980). See figure caption 7 for details. The solid hexagon denotes values of $a_{Ca^{+2}}/a^2_{H^+}$ and $a_{Fe^{+3}}/a^3_{H^+}$ in the geothermal reservoir compatible with measured compositions of epidote and prehnite solid solutions from well M84 at 1470 meters depth (see Table 2).

Figure 20. Theoretical activity-activity phase diagram for the system $CaO-MgO-Al_2O_3-SiO_2-H_2O$ at 312°C and 104 bars in the presence of quartz and an aqueous solutions in which $a_{H_2O} = 1$. Broken curves denote saturation in the fluid phase with the labeled phase. Diagram A illustrates phase relations for stoichiometric minerals and diagram B is constructed for the observed phase relations of epidote and pyroxene solid solutions from well T366 at 2655 meters

depth (Table 2). Compositions and activities of garnet and prehnite solid solutions are calculated from equations and data given by Bird and Helgeson (1980) and equation (9) for the composition of epidote reported in Table 2 for well T366 at 2655 m. Compositions of tremolite solid solution used in diagram B is also given in Table 2. The open symbol represents values of a_{Ca++}/a^2_{H+} and a_{Mg++}/a^2_{H+} in the geothermal reservoir fluid compatible with the measured epidote and clinopyroxene solid solutions from well T366 at 2655 meters depth. See text and figure caption 7 for details.

Figure 21. Calculated values of $a_{Ca}{}^{++}/a^2_{H}{}^{+}$ in Cerro Prieto geothermal fluids. Circles represent values based on coexisting epidote and prehnite using reaction (8). Hexagon (21B) based on coexisting biotite+K-feldspar+pyroxene using reaction (12). Rectangles represent the range in values bounded by the prehnite-limiting (8) and tremolite-limiting (10) reactions. Activity-composition relations are from Bird and Helgeson (1980), Bird and Norton (1981), and as described in text. Where the required composition of coexisting tremolite was not available at a given depth, mineral compositions from adjacent depth were used (see Table 2).

Figure 22. Calculated values (open symbols) of log a_{Ca++}/a_{Mg++} in Cerro Prieto geothermal fluids coexisting with epidote and clinopyroxene solid solutions (Table 2) as a function of temperature (diagram A) and epidote composition (diagram B). Maximum values of a_{Ca++}/a_{Mg++} are calculated from the mass action equation for reactions (8) and (9) and denote the prehnite limiting reactions, and minimum values of a_{Ca++}/a_{Mg++} are calculated from the mass action equations for reactions (10) and (11) and represent the tremolite limiting reactions. Values for well M84 are for only prehnite limiting reactions. Measured (solid symbols) values of a_{Ca++}/a_{Mg++} in Cerro Prieto geothermal reservoir fluids are given in Diagram A as computed from data reported by Fausto

(1979) with the approximation that $\gamma_{Ca^{++}}/\gamma_{Mg^{++}} \sim 1$; fluid temperatures obtained by silica geothermometry (see figure caption 7 for details).

Figure 23. Calculated values of log f_{O_2} in Cerro Prieto geothermal reservoir fluids coexisting with epidote-clinopyroxene solid solutions (Table 2) as a function of epidote composition (diagram A) and temperature (diagram B). Open symbols are computed from mass action equations for reactions (10), (12) and (15) (see text). Solid curves in diagram B denote common f_{O_2} buffers in the system FeO-Fe_2O_3-SiO_2. The filled circle is value of log f_{O_2} calculated by Bird and Norton (1981), for the assemblage of biotite, epidote, tremolite, quartz and an aqueous solution from the Elmore #1 well in the Salton Sea geothermal system.

TABLE 1

Occurrences of Hydrothermal Calc-Silicate Minerals
in Selected Active Geothermal Systems

System[a]	Heulandite	Laumontite	Wairakite	Prehnite	Epidote	Amphibole	Calcium Clino-Pyroxene	Garnet	Wollastonite	Sphene	Calc-Silicate Host Rock	Geothermal[b] Fluid Type
Otake, Japan		X	X		X						Andesite	A3
Onikobe, Japan		X	X								Andesite	A1, D
Yugawara, Japan		X	X								Basalt and Andesite	A3
Matsukawa, Japan		X									Andesite	C
Tatun, Taiwan		X	X		X					X	Andesite	D
Tongonan, Philippines	X	X	X	X	X	X		X	X	X	Andesite	A2
Broadlands, New Zealand	X		X		X						Rhyolite	A3
Wairakei, New Zealand	?	X	X	X	X						Rhyolite	A3
Kamchatka, U.S.S.R.		X	X	X	X	X		X			Andesite	A3
Low Temperature, Iceland	X	X									Basalt	A3
High Temperature, Iceland	X	X	X	X	X	X		X	X		Basalt	A3, A1
Larderello, Italy			X	X	X	X	X	X	X	X	Metamorphic and Sedimentary	B
Geysers, U.S.A.			X	X	X	X	?	X		X	Metagreywacke and Metabasalt	B
Yellowstone, U.S.A.	X	X	X								Rhyolite	A3
Salton Sea, U.S.A.					X	X	X	X		X	Sandstone	A1
Heber, U.S.A.			X	X	X					X	Diabase	A2
Cerro Prieto, Mexico			X	X	X	X	X			X	Sandstone	A2

(a) References - Otake: Hayashi and Yamasaki, 1976; Onikobe: Seki et al., 1969; Yamada, 1976; Yugawara: Oki et al., 1976; Matsukawa: Sumi, 1965; Tatun: Lan et al., 1980; Tongonan: Ferrer, 1983; Broadlands: Browne and Ellis, 1970; Wairakei: Steiner, 1977; Kamchatka: Naboko, 1970, 1976; White and Sigvaldason, 1962; Iceland: Kristmannsdottir, 1981; Kristmannsdottir and Tomasson, 1976, 1978; Sigvaldason, 1962; Tomasson and Kristmannsdottir, 1972, 1976; Larderello: Cavarretta et al., 1980, 1982; Geysers: Steiner, 1958; Lockner et al., 1982; Sternfeld, 1981; Yellowstone: Baragar and Beeson, 1981; Salton Sea: Helgeson, 1967; Keith et al., 1968; Kendall, 1976; Tewey, 1977; Muffler and White, 1969; McDowell and McCurry, 1977; McDowell (pers. comm.), 1982; Heber: Browne, 1977; Cerro Prieto: Reed, 1976; Elders et al., 1981; this study.

(b) Type of geothermal reservoir fluids: A1 = alkali chloride (TDS > 100,000 ppm); A2 = alkali chloride (100,000 ppm < TDS > 10,000 ppm); A3 = alkali chloride (TDS < 10,000 ppm); B = steam field; C = acid sulfate; D = acid sulfate-chloride. Modified after Ellis and Mahon, 1977.

TABLE 2

Compositions of Coexisting Minerals Used in Thermochemical Calculations

									Clinopyroxene			K-Spar	
Well	Depth (m)	Temp[a] (°C)	Cutting[b]	$X^{EP(c,d)}$	X^{PR}	X^{HR}	X^{BI}	X^{ACT}	WO	EN	FS	AB	OR
M-48	1199	323	VEIN	0.236	0.179	--	--	--	--	--	--	--	--
M-53	1797	309	SLS	0.164	--	--	--	--	--	--	--	5.4	94.5
	1842	318	SLS	0.138	--	0.98	--	--	--	--	--	--	--
	1905	328	SLS	0.237	--	--	0.68	0.62	--	--	--	--	--
	1935	331	SLS	0.213	--	--	0.59	--	--	--	--	--	--
			SLS	--	--	--	0.68	0.65	--	--	--	--	--
	1974	335	SLS	0.167	--	--	0.84	--	--	--	--	--	--
			SLS	0.187	--	--	0.76	--	--	--	--	--	--
M-84	1284	321	SS	0.192	--	1.00	--	--	--	--	--	--	--
	1299	322	SS	0.159	--	--	--	--	--	--	--	4.4	95.6
			SS	0.169	--	--	--	--	--	--	--	3.3	96.7
	1470	334	SS	0.204	0.082	--	--	--	--	--	--	--	--
	1497	336	SS	0.187	0.086	--	--	--	--	--	--	--	--
	1557	339	SS	0.252	0.150	--	--	.078	--	--	--	--	--
			SS	0.199	0.069	--	--	--	--	--	--	--	--
			SS	0.253	0.082	--	--	--	48.7	30.1	21.2	--	--
			SS	0.237	0.153	--	--	--	--	--	--	--	--
			SS	0.237	0.134	--	--	--	49.4	29.3	21.3	--	--
	1656	344	SS	0.203	0.155	--	--	--	--	--	--	--	--
			SS	0.210	0.044	--	--	--	--	--	--	--	--
M-93	2391	325	SS	0.197	0.055	--	--	--	--	--	--	5.2	94.7
	2424	330	SS	0.168	--	--	--	0.73	50.5	18.5	31.0	--	--
			SS	0.175	--	--	--	--	49.0	18.0	33.0	--	--
	2454	335	SS	0.254	--	--	--	--	--	--	--	5.4	94.6
			SS	--	--	--	--	--	50.0	23.0	27.0	4.1	95.9

(a) Downhole temperatures are interpolated from temperature logs supplied by La Comisión Federal de Electricidad (M-48: Log T-17; M-53: Log T-25; M-84: Log T-12; M-125: Log T-8; T-366: Log T-22). M-93 temperature from Bermejo et al., 1979.

(b) Abbreviations: SLS = siltstone; SS = sandstone.

(c) Abbreviations: X^{EP}, $X^{PR} = Fe^{+3}/Fe^{+3}+Al^{VI}$

$X^{HR} = Ca/Na+K+Ca$

X^{BI}, $X^{ACT} = Mg/Fe+Mn+Mg$

(d) Mineral composition analyses were conducted on an automated MAC electron microprobe at the California Institute of Technology. Both wavelength dispersive and energy dispersive systems were employed. All corrections were accomplished using simple silicate mineral standards and Bence-Albee (1968) procedures. Designation of "coexisting" minerals implies that they occur in the same cutting from a given depth interval of a specific well, although they are not necessarily in physical contact.

TABLE 2 (continued)

Compositions of Coexisting Minerals Used in Thermochemical Calculations

									Clinopyroxene			K-Spar	
Well	Depth (m)	Temp[a] (°C)	Cutting[b]	$x^{EP(c,d)}$	x^{PR}	x^{WR}	x^{BI}	x^{ACT}	WO	EN	FS	AB	OR
M-125	2019	349	SS	0.174	0.078	--	--	--	--	--	--	--	--
	2100	348	SS	0.196	0.064	--	--	--	--	--	--	4.9	95.1
			SS	0.198	0.108	--	--	0.68	--	--	--	--	--
	2241	340	SS	--	--	--	0.66	--	--	--	--	7.1	92.9
			SS	0.246	--	--	0.65	--	50.0	22.0	28.0	--	--
	2280	336	SS	0.225	--	--	--	--	49.4	27.5	23.1	--	--
	2310	335	SS	0.205	--	--	0.75	--	--	--	--	--	--
	2319	335	SS	0.225	--	--	0.73	--	--	--	--	4.2	95.8
			SS	0.169	0.065	--	--	--	--	--	--	--	--
T-366	2655	312	SS	0.168	--	--	--	--	49.1	28.4	22.5	--	--
			SS	0.179	--	--	--	0.82	--	--	--	--	--
	2736	315	SS	0.192	--	--	--	--	47.9	40.1	11.9	--	--
			SS	0.200	--	--	--	--	48.0	30.2	21.8	--	--
	2850	320	SS	--	--	--	--	--	49.3	17.1	33.6	5.4	94.6
			SS	--	0.046	--	--	--	49.4	44.9	5.7	--	--
	2985	325	SS	--	--	--	--	--	48.6	34.8	16.6	5.2	94.8
			SS	0.197	0.040	--	--	--	--	--	--	--	--

(a) (b) (c) (d) are explained on previous page.

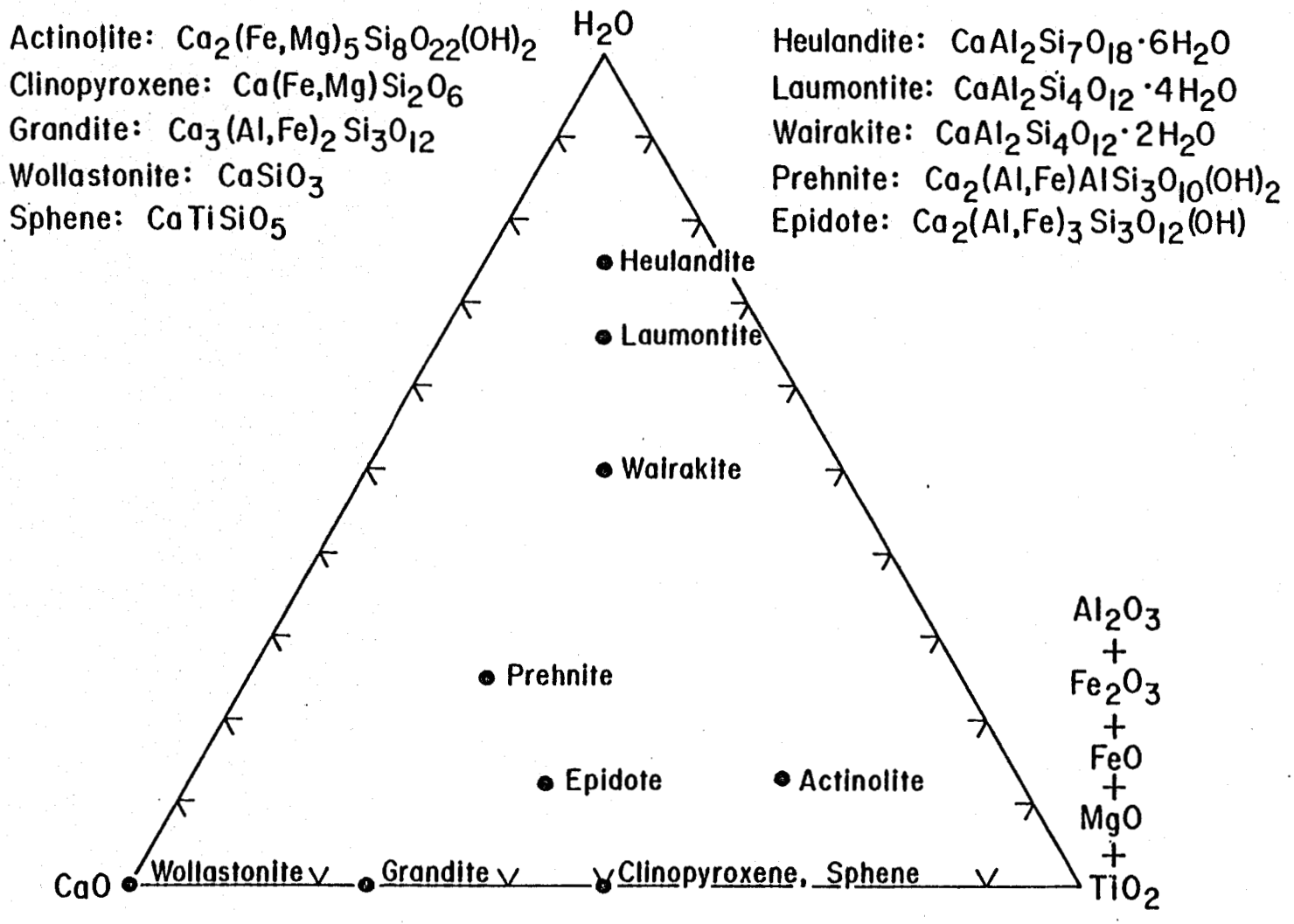
Actinolite: $Ca_2(Fe,Mg)_5Si_8O_{22}(OH)_2$
Clinopyroxene: $Ca(Fe,Mg)Si_2O_6$
Grandite: $Ca_3(Al,Fe)_2Si_3O_{12}$
Wollastonite: $CaSiO_3$
Sphene: $CaTiSiO_5$
H_2O
Heulandite: $CaAl_2Si_7O_{18}\cdot 6H_2O$
Laumontite: $CaAl_2Si_4O_{12}\cdot 4H_2O$
Wairakite: $CaAl_2Si_4O_{12}\cdot 2H_2O$
Prehnite: $Ca_2(Al,Fe)AlSi_3O_{10}(OH)_2$
Epidote: $Ca_2(Al,Fe)_3Si_3O_{12}(OH)$
Heulandite
Laumontite
Wairakite
Prehnite
Epidote
Actinolite
Al_2O_3 + Fe_2O_3 + FeO + MgO + TiO_2
CaO
Wollastonite
Grandite
Clinopyroxene, Sphene

Figure 1.

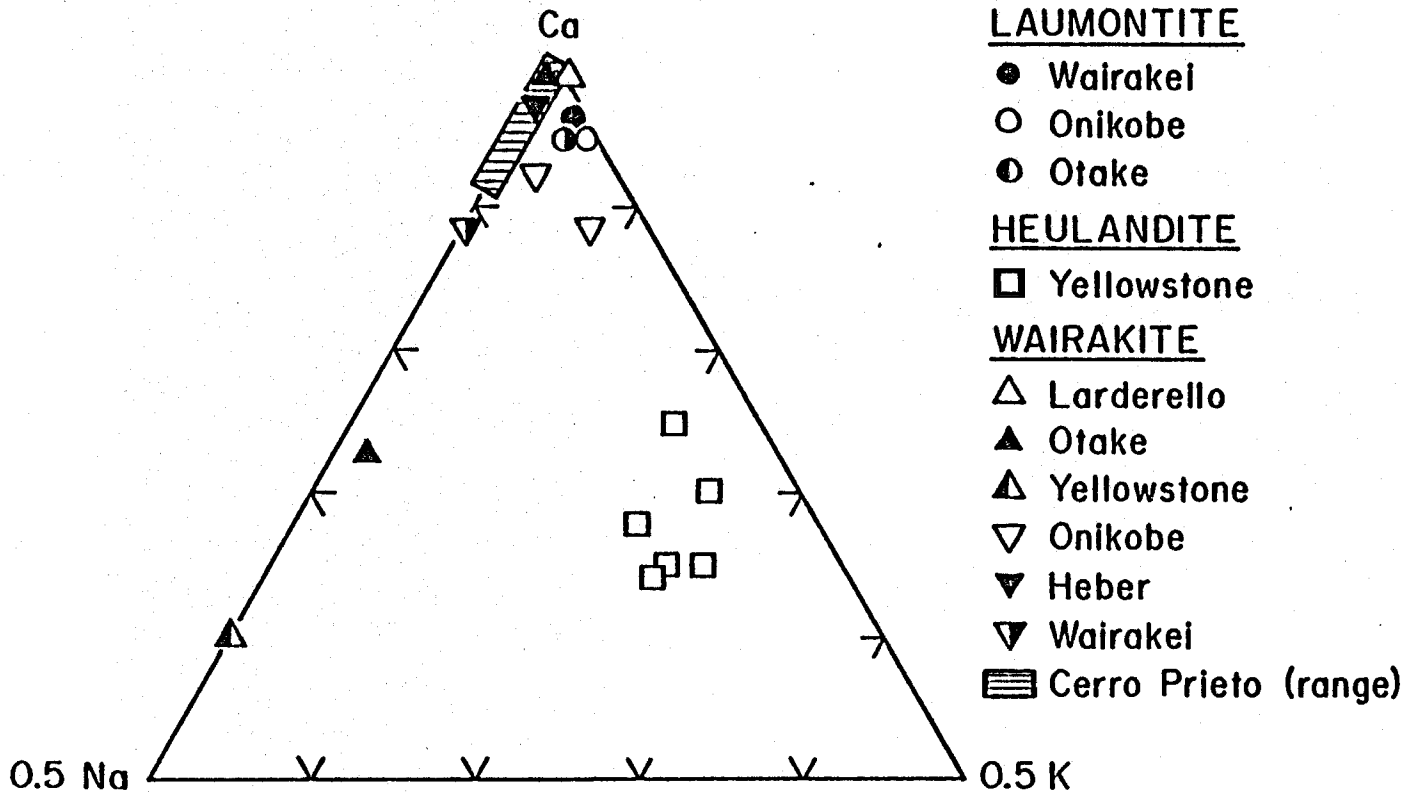
Ca
0.5 Na
0.5 K
LAUMONTITE
Wairakei
Onikobe
Otake
HEULANDITE
Yellowstone
WAIRAKITE
Larderello
Otake
Yellowstone
Onikobe
Heber
Wairakei
Cerro Prieto (range)

Figure 2.

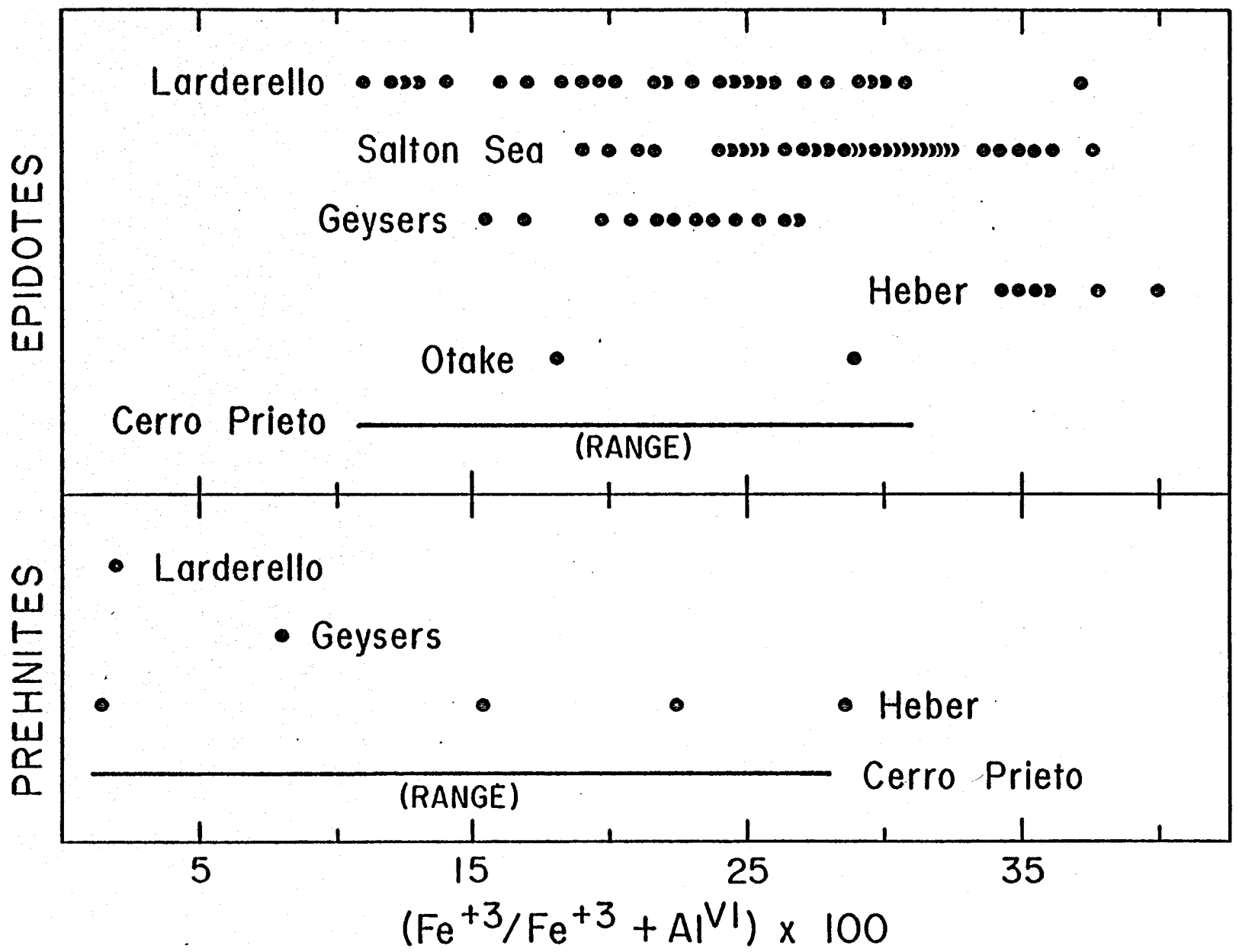
EPIDOTES
Larderello
Salton Sea
Geysers
Heber
Otake
Cerro Prieto
(RANGE)
PREHNITES
Larderello
Geysers
Heber
Cerro Prieto
(RANGE)
5
15
25
35
(Fe+3/Fe+3 + AlVI) x 100

Figure 3.

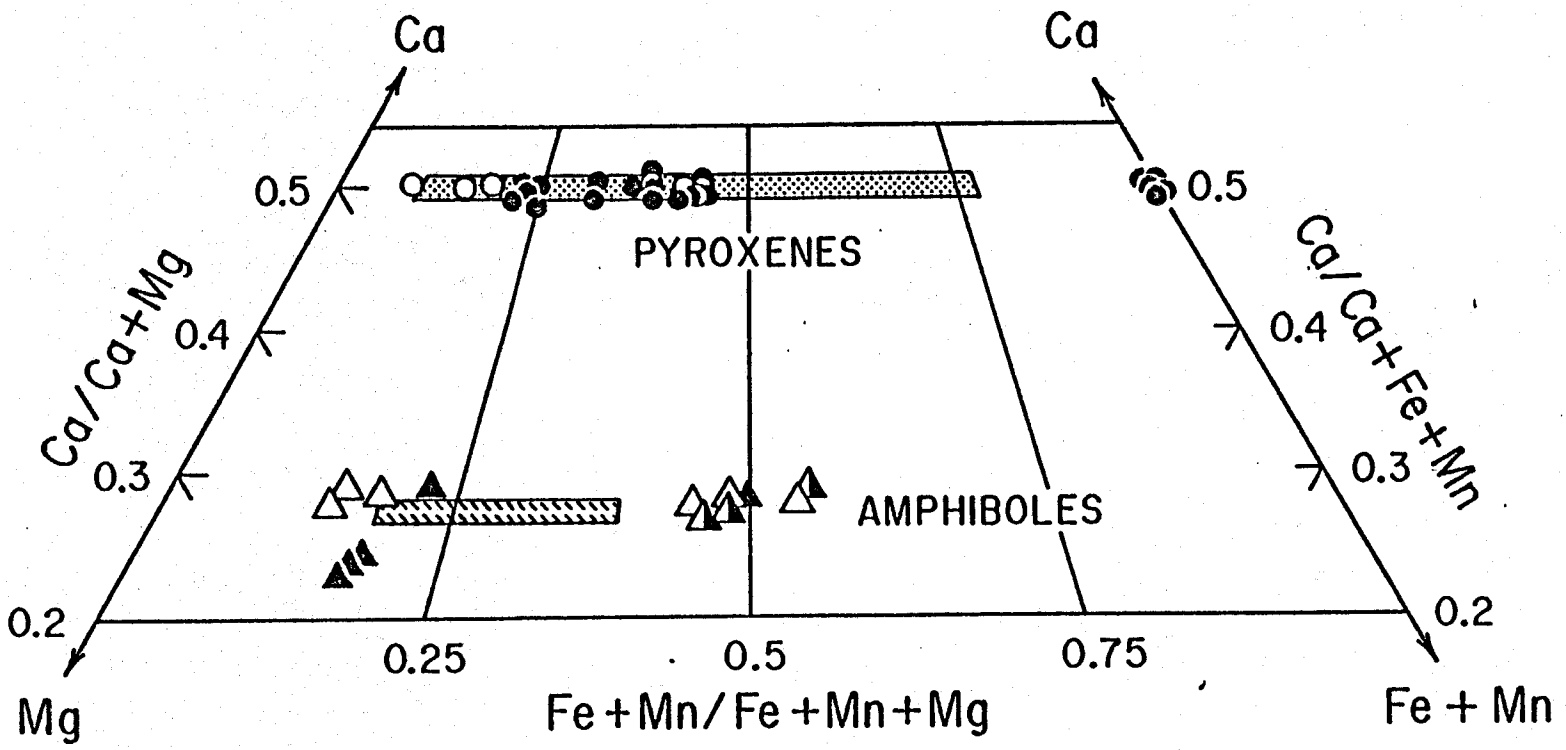

PYROXENES

- SALTON SEA
- LARDERELLO
- CERRO PRIETO

AMPHIBOLES

- SALTON SEA
- LARDERELLO
- GEYSERS
- CERRO PRIETO

Figure 4A.

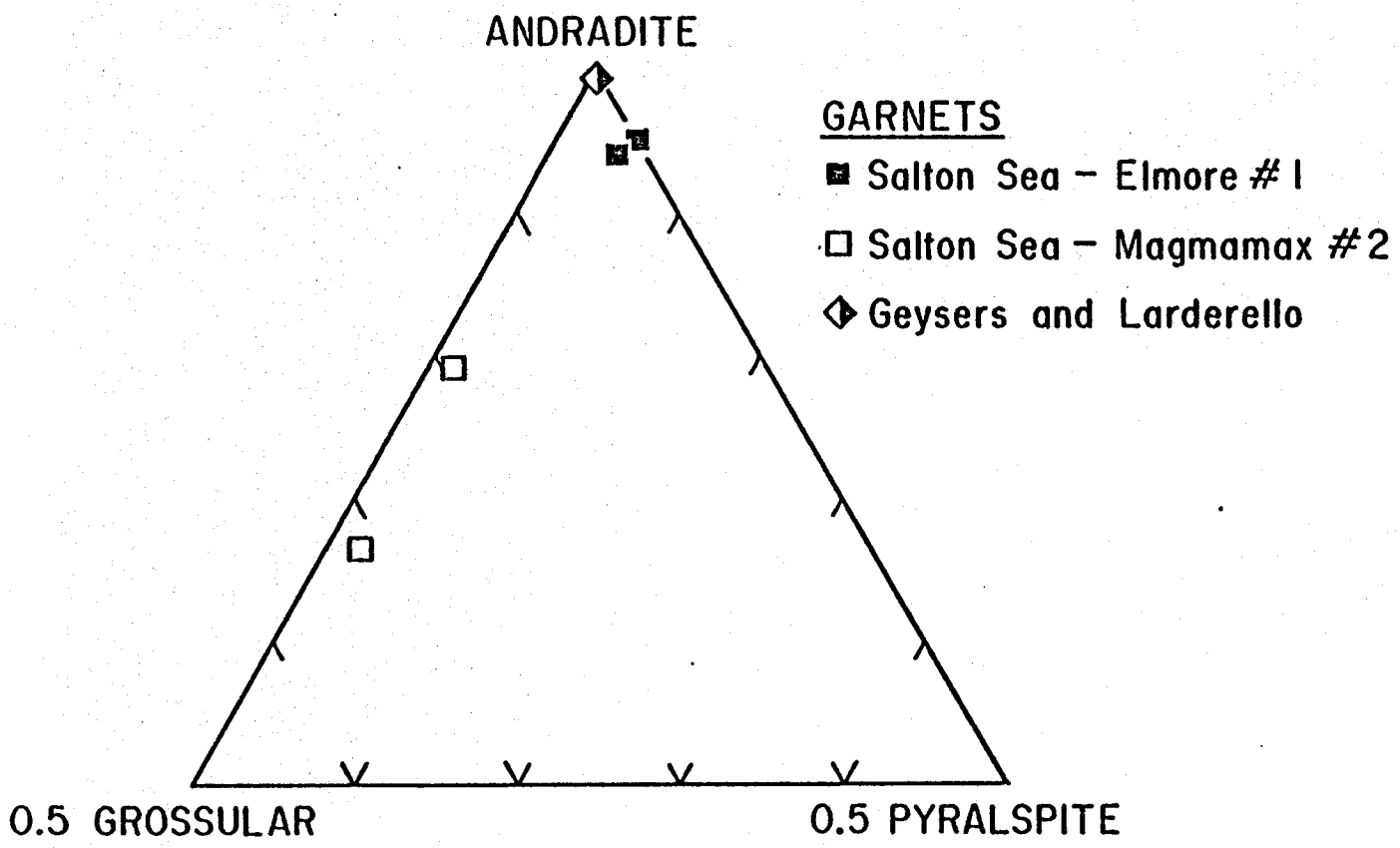
ANDRADITE
GARNETS
Salton Sea – Elmore #1
Salton Sea – Magmamax #2
Geysers and Larderello
0.5 GROSSULAR
0.5 PYRALSPITE

Figure 4B.

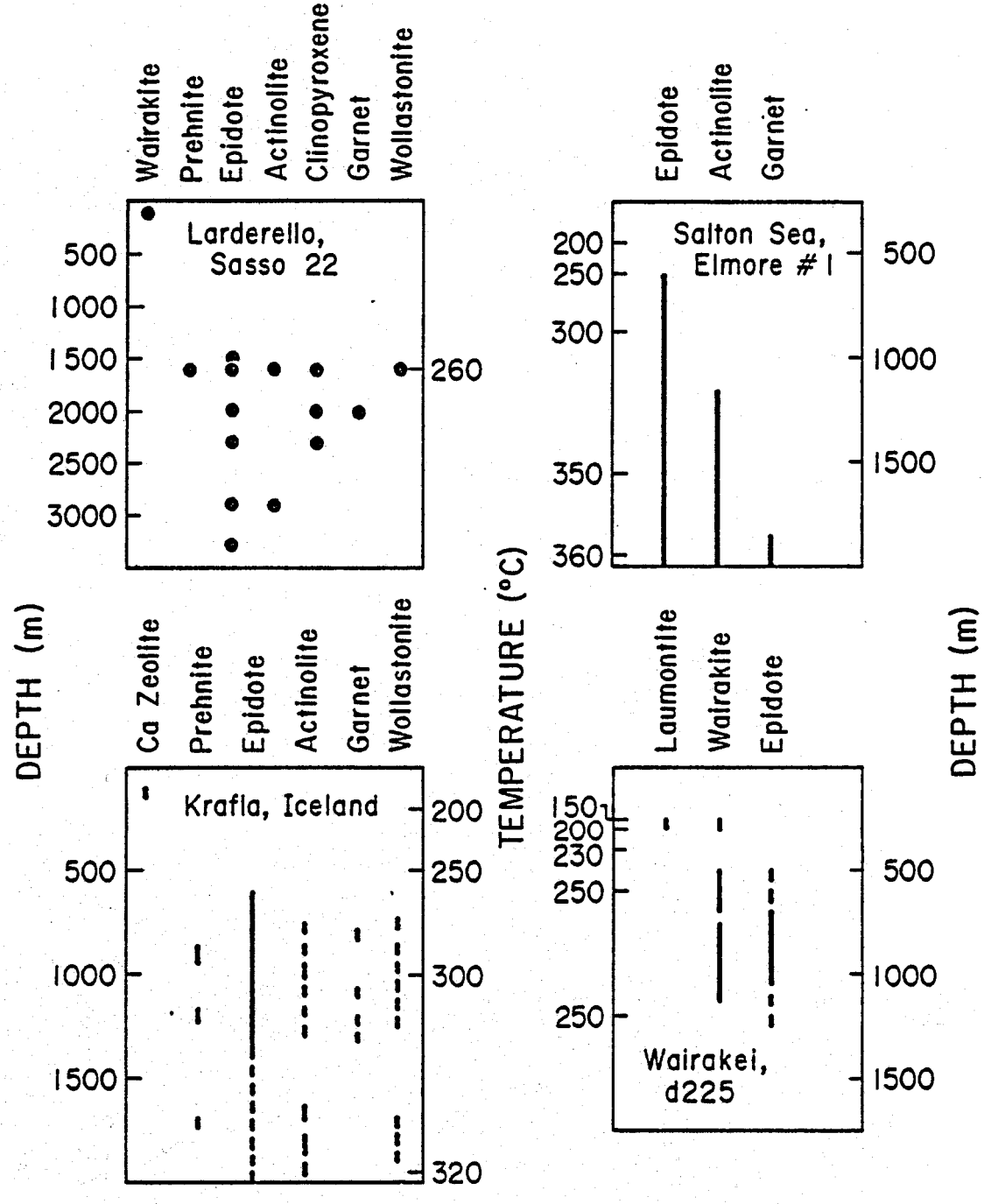
Wairakite
Prehnite
Epidote
Actinolite
Clinopyroxene
Garnet
Wollastonite
Larderello,
Sasso 22
500
1000
1500
2000
2500
3000
260
Epidote
Actinolite
Garnet
Salton Sea,
Elmore #1
200
250
300
350
360
500
1000
1500
DEPTH (m)
TEMPERATURE (°C)
Ca Zeolite
Prehnite
Epidote
Actinolite
Garnet
Wollastonite
Krafla, Iceland
500
1000
1500
200
250
300
320
Laumontite
Wairakite
Epidote
150
200
230
250
250
Wairakei,
d225
500
1000
1500
DEPTH (m)

Figure 5.

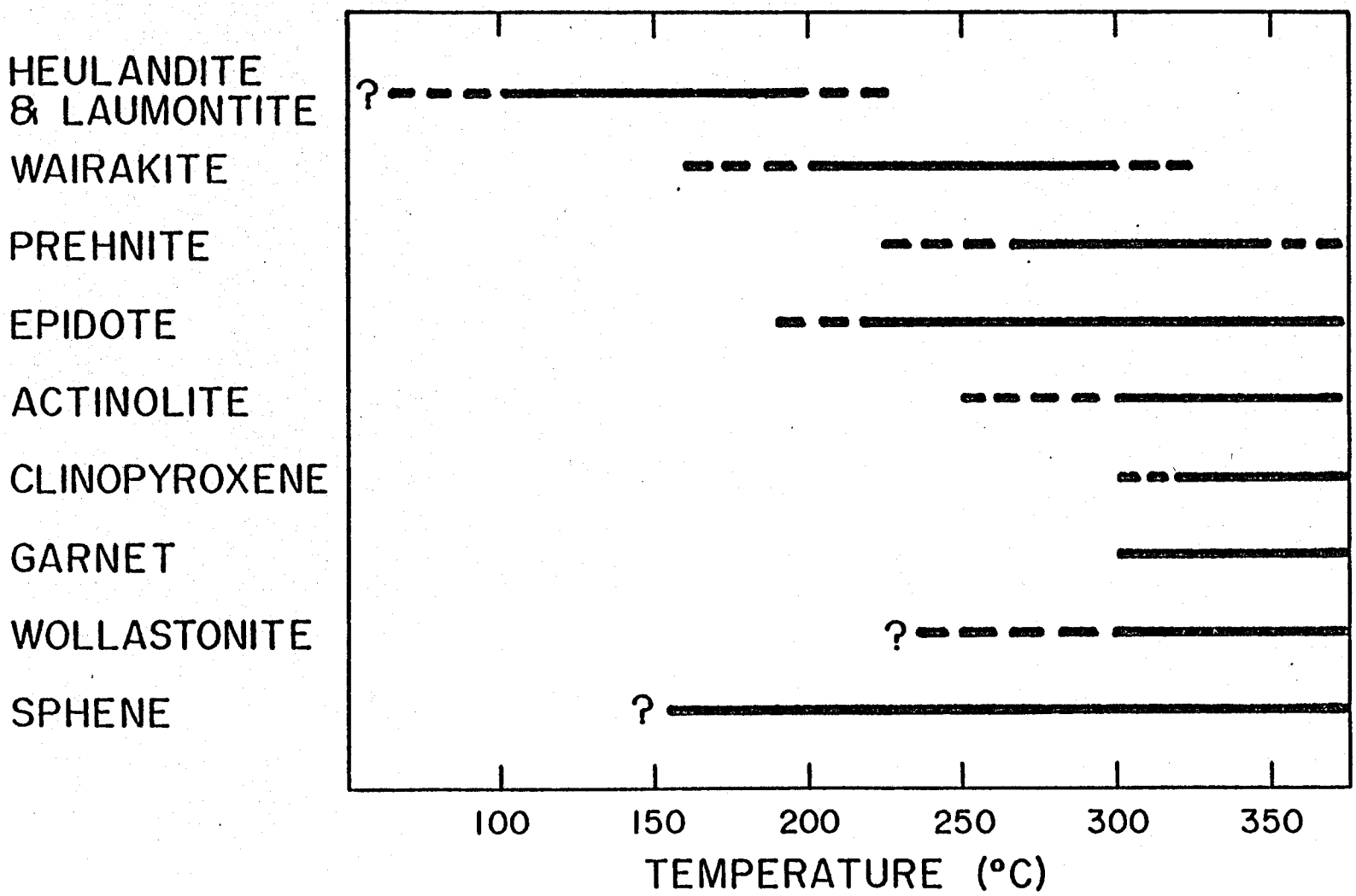
HEULANDITE
& LAUMONTITE
WAIRAKITE
PREHNITE
EPIDOTE
ACTINOLITE
CLINOPYROXENE
GARNET
WOLLASTONITE
SPHENE
?
?
?
100
150
200
250
300
350
TEMPERATURE (°C)

Figure 6.

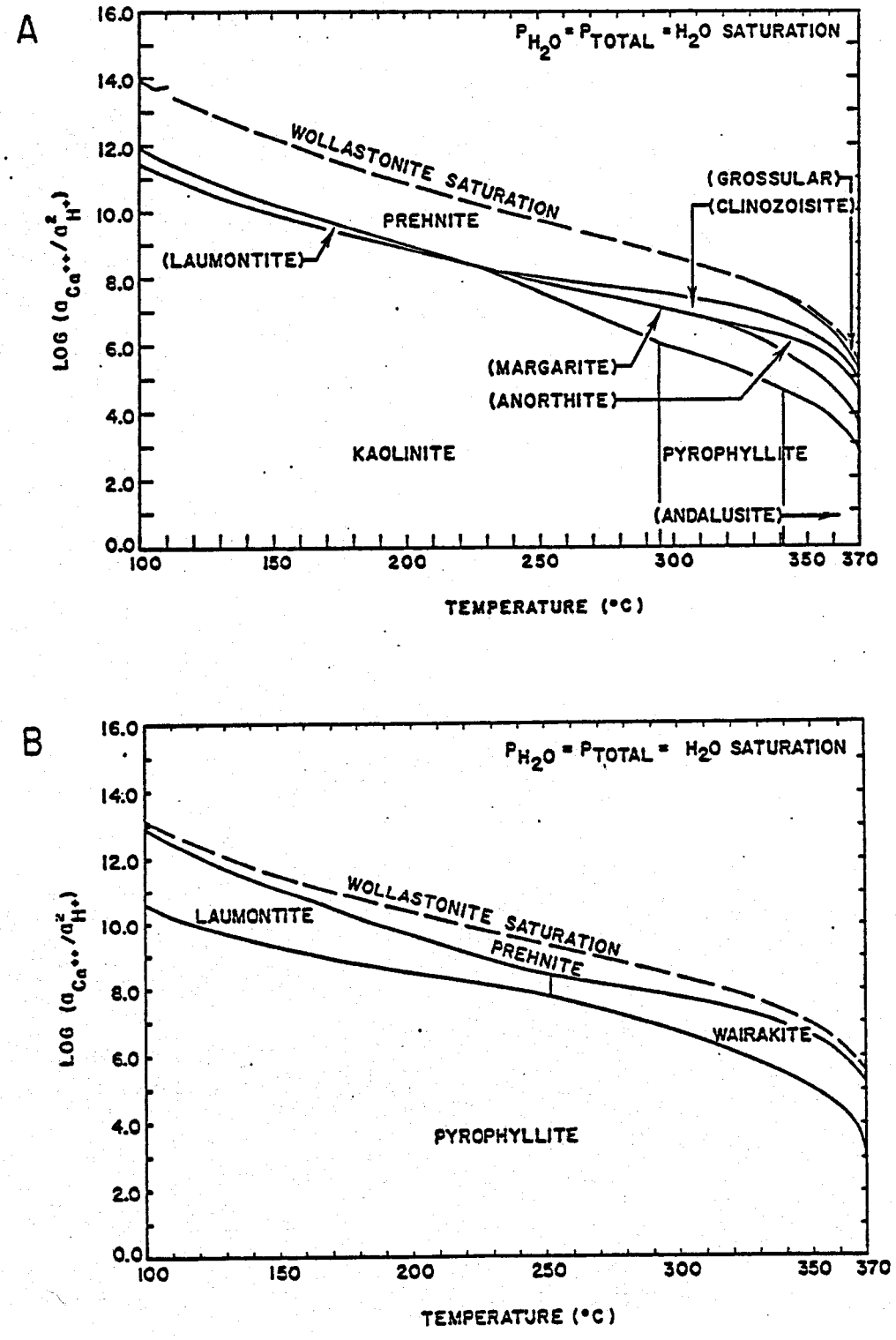
A
$P_{H_2O} = P_{TOTAL} = H_2O$ SATURATION
WOLLASTONITE SATURATION
PREHNITE
(LAUMONTITE)
(GROSSULAR)
(CLINOZOISITE)
(MARGARITE)
(ANORTHITE)
KAOLINITE
PYROPHYLLITE
(ANDALUSITE)
LOG ($a_{Ca^{++}}/a^2_{H^+}$)
TEMPERATURE (°C)
B
$P_{H_2O} = P_{TOTAL} = H_2O$ SATURATION
WOLLASTONITE SATURATION
LAUMONTITE
PREHNITE
WAIRAKITE
PYROPHYLLITE
LOG ($a_{Ca^{++}}/a^2_{H^+}$)
TEMPERATURE (°C)

Figure 7.

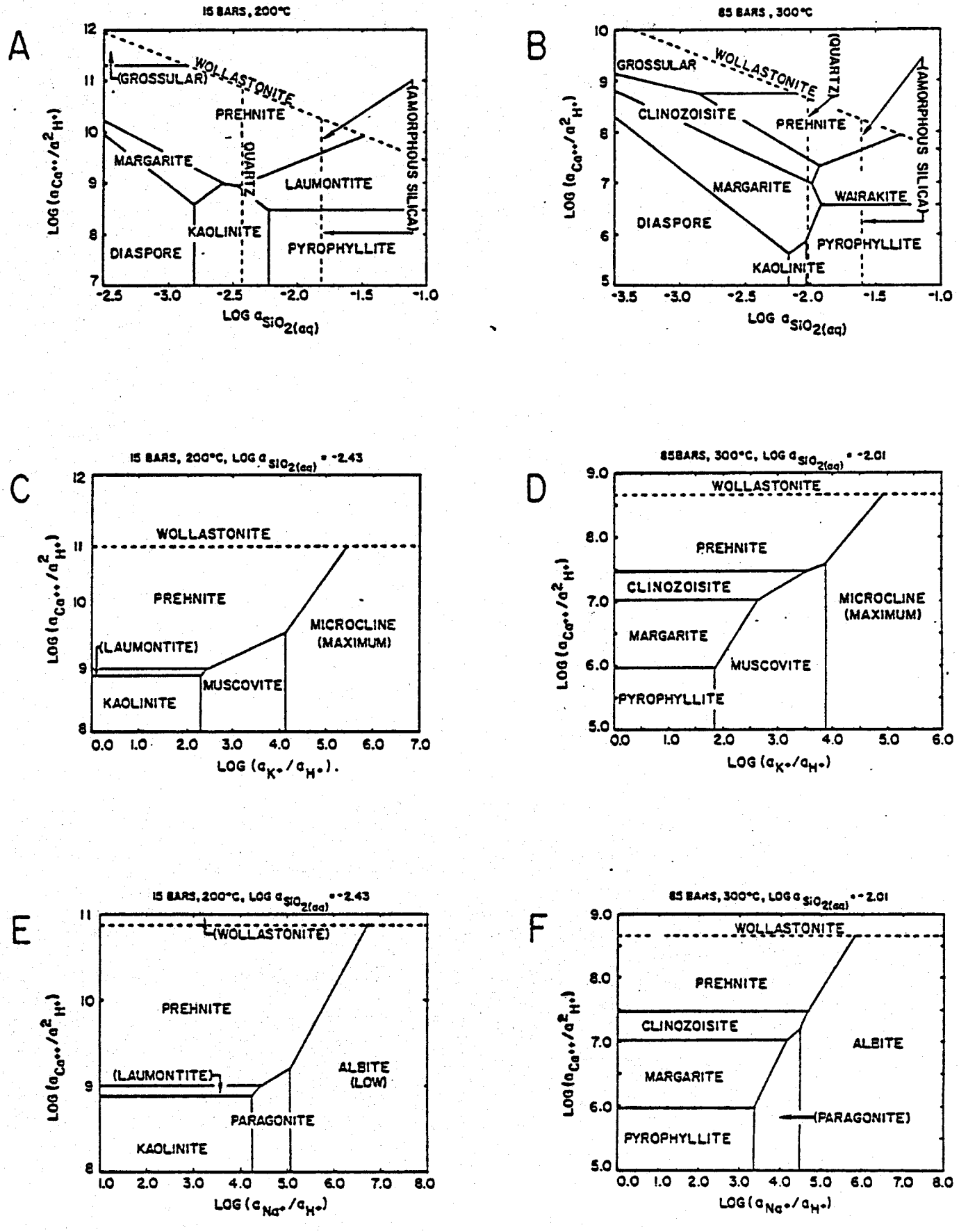
A
15 BARS, 200°C
(GROSSULAR)
WOLLASTONITE
PREHNITE
MARGARITE
QUARTZ
LAUMONTITE
(AMORPHOUS SILICA)
KAOLINITE
DIASPORE
PYROPHYLLITE
LOG (aCa++/a2H+)
LOG aSiO2(aq)
B
85 BARS, 300°C
GROSSULAR
WOLLASTONITE
(QUARTZ)
(AMORPHOUS SILICA)
CLINOZOISITE
PREHNITE
MARGARITE
WAIRAKITE
DIASPORE
PYROPHYLLITE
KAOLINITE
C
15 BARS, 200°C, LOG aSiO2(aq) = -2.43
WOLLASTONITE
PREHNITE
(LAUMONTITE)
MICROCLINE (MAXIMUM)
MUSCOVITE
KAOLINITE
LOG (aK+/aH+)
D
85BARS, 300°C, LOG aSiO2(aq) = -2.01
WOLLASTONITE
PREHNITE
CLINOZOISITE
MICROCLINE (MAXIMUM)
MARGARITE
MUSCOVITE
PYROPHYLLITE
LOG (aK+/aH+)
E
15 BARS, 200°C, LOG aSiO2(aq) = -2.43
(WOLLASTONITE)
PREHNITE
(LAUMONTITE)
ALBITE (LOW)
PARAGONITE
KAOLINITE
LOG (aNa+/aH+)
F
85 BARS, 300°C, LOG aSiO2(aq) = -2.01
WOLLASTONITE
PREHNITE
CLINOZOISITE
ALBITE
MARGARITE
(PARAGONITE)
PYROPHYLLITE
LOG (aNa+/aH+)

Figure 8.

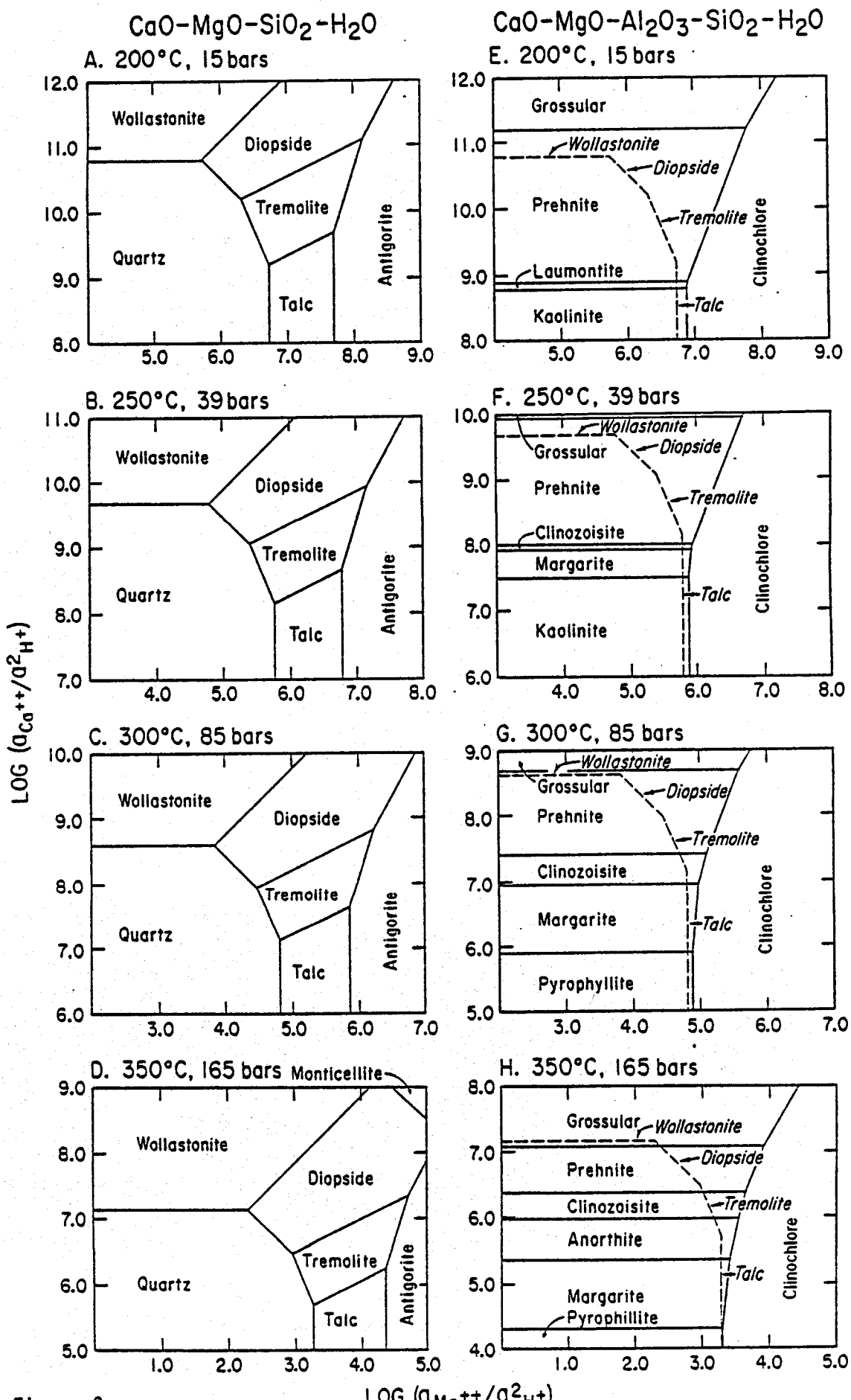
CaO-MgO-SiO2-H2O
A. 200°C, 15 bars
Wollastonite
Diopside
Tremolite
Quartz
Talc
Antigorite
B. 250°C, 39 bars
C. 300°C, 85 bars
D. 350°C, 165 bars
Monticellite
CaO-MgO-Al2O3-SiO2-H2O
E. 200°C, 15 bars
Grossular
Prehnite
Laumontite
Kaolinite
Clinochlore
F. 250°C, 39 bars
Clinozoisite
Margarite
G. 300°C, 85 bars
Pyrophyllite
H. 350°C, 165 bars
Anorthite
Pyrophillite
LOG (aCa++/a2H+)
LOG (aMg++/a2H+)

Figure 9.

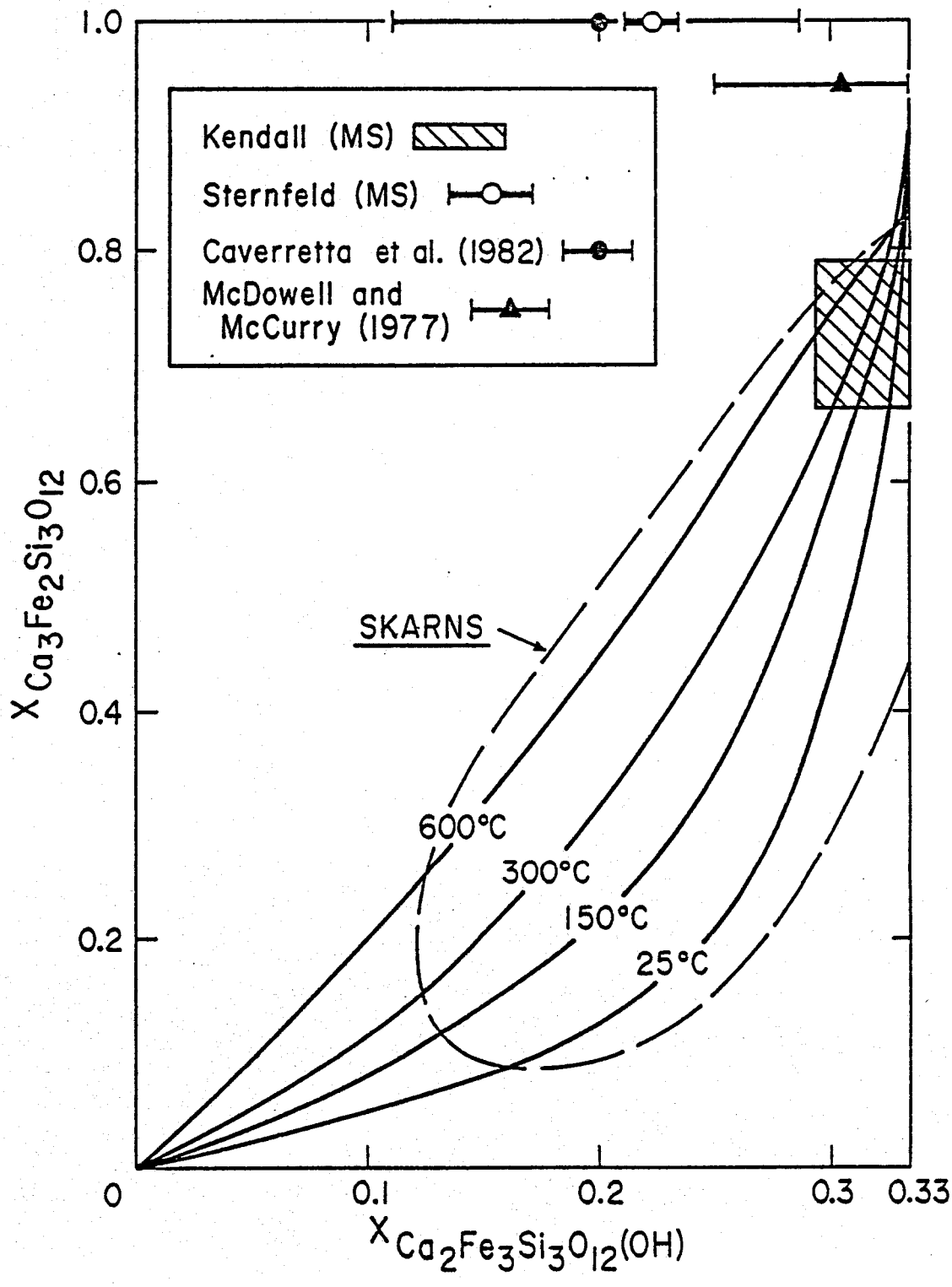
1.0
0.8
0.6
0.4
0.2
0
0.1
0.2
0.3
0.33
Kendall (MS)
Sternfeld (MS)
Caverretta et al. (1982)
McDowell and McCurry (1977)
SKARNS
600°C
300°C
150°C
25°C
$X_{Ca_3Fe_2Si_3O_{12}}$
$X_{Ca_2Fe_3Si_3O_{12}(OH)}$

Figure 10.

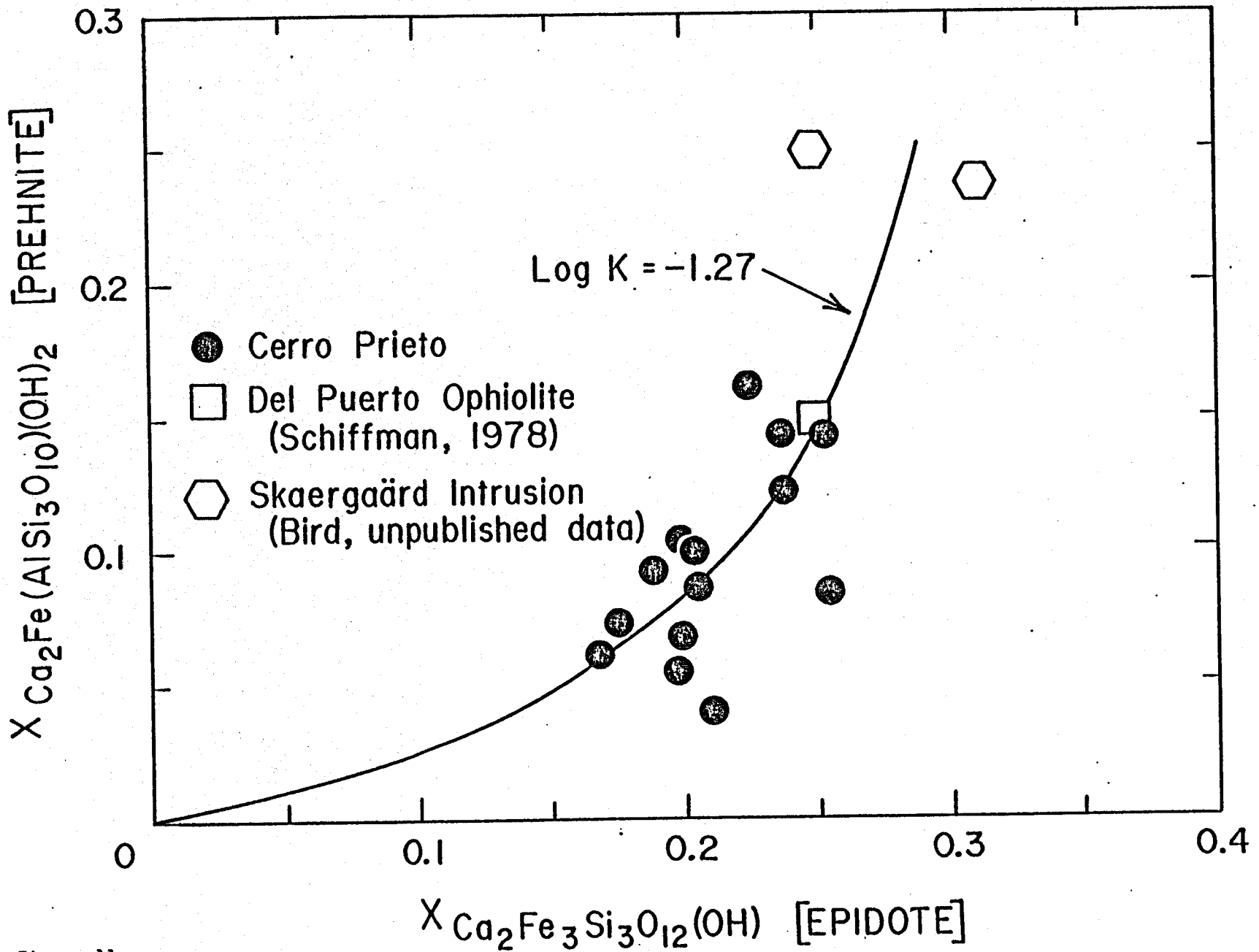
0.3
0.2
0.1
0
0.1
0.2
0.3
0.4
X Ca2Fe(AlSi3O10)(OH)2 [PREHNITE]
X Ca2Fe3Si3O12(OH) [EPIDOTE]
Log K = -1.27
Cerro Prieto
Del Puerto Ophiolite
(Schiffman, 1978)
Skaergaärd Intrusion
(Bird, unpublished data)

Figure 11.

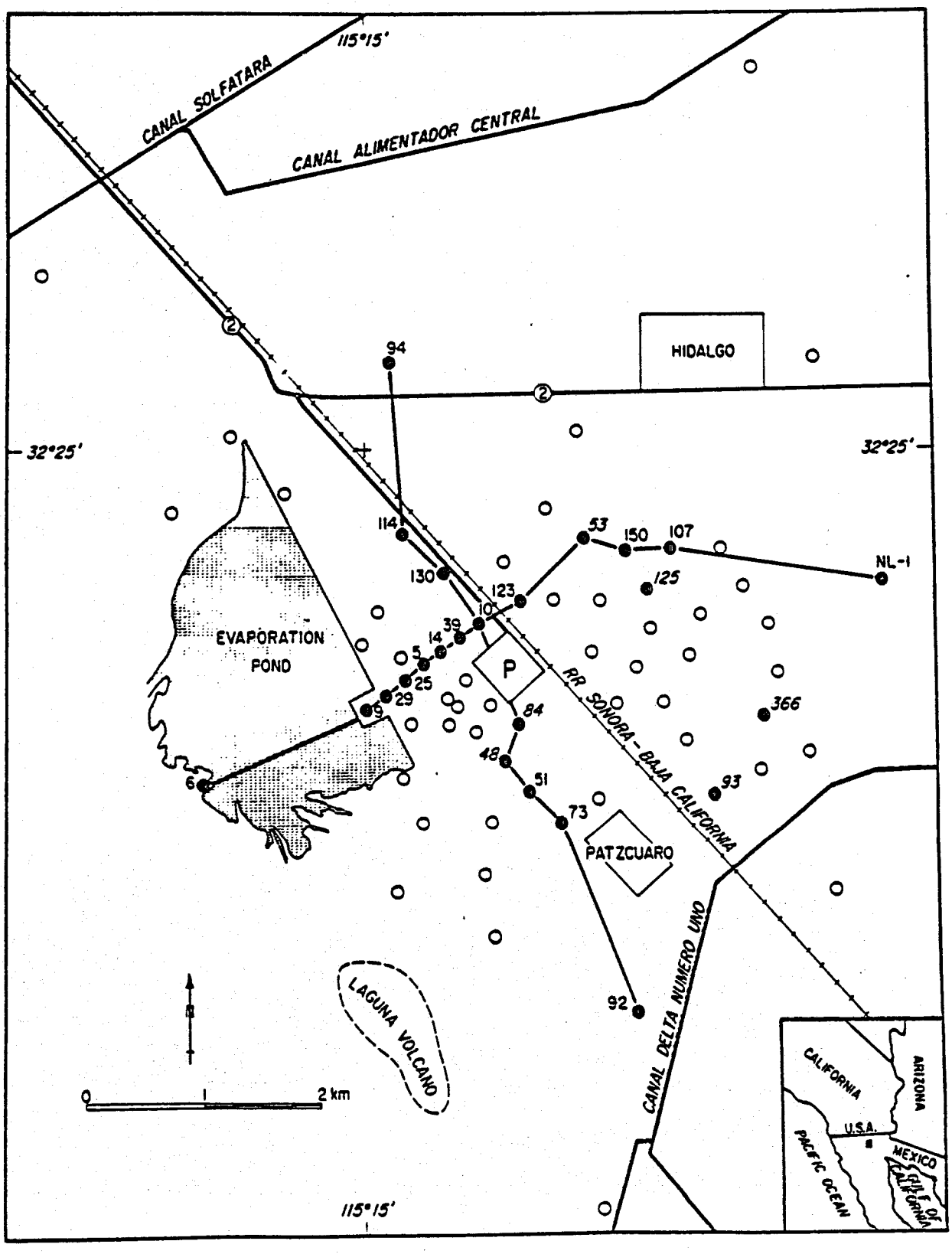
CANAL SOLFATARA
115°15'
CANAL ALIMENTADOR CENTRAL
HIDALGO
94
32°25'
32°25'
114
130
53
150
107
NL-1
125
123
10
39
14
5
25
29
9
6
EVAPORATION
POND
P
RR SONORA - BAJA CALIFORNIA
366
84
48
51
73
93
PATZCUARO
92
CANAL DELTA NUMERO UNO
LAGUNA VOLCANO
N
0
1
2 km
CALIFORNIA
ARIZONA
U.S.A.
MEXICO
PACIFIC OCEAN
GULF OF CALIFORNIA
115°15'

Figure 12.

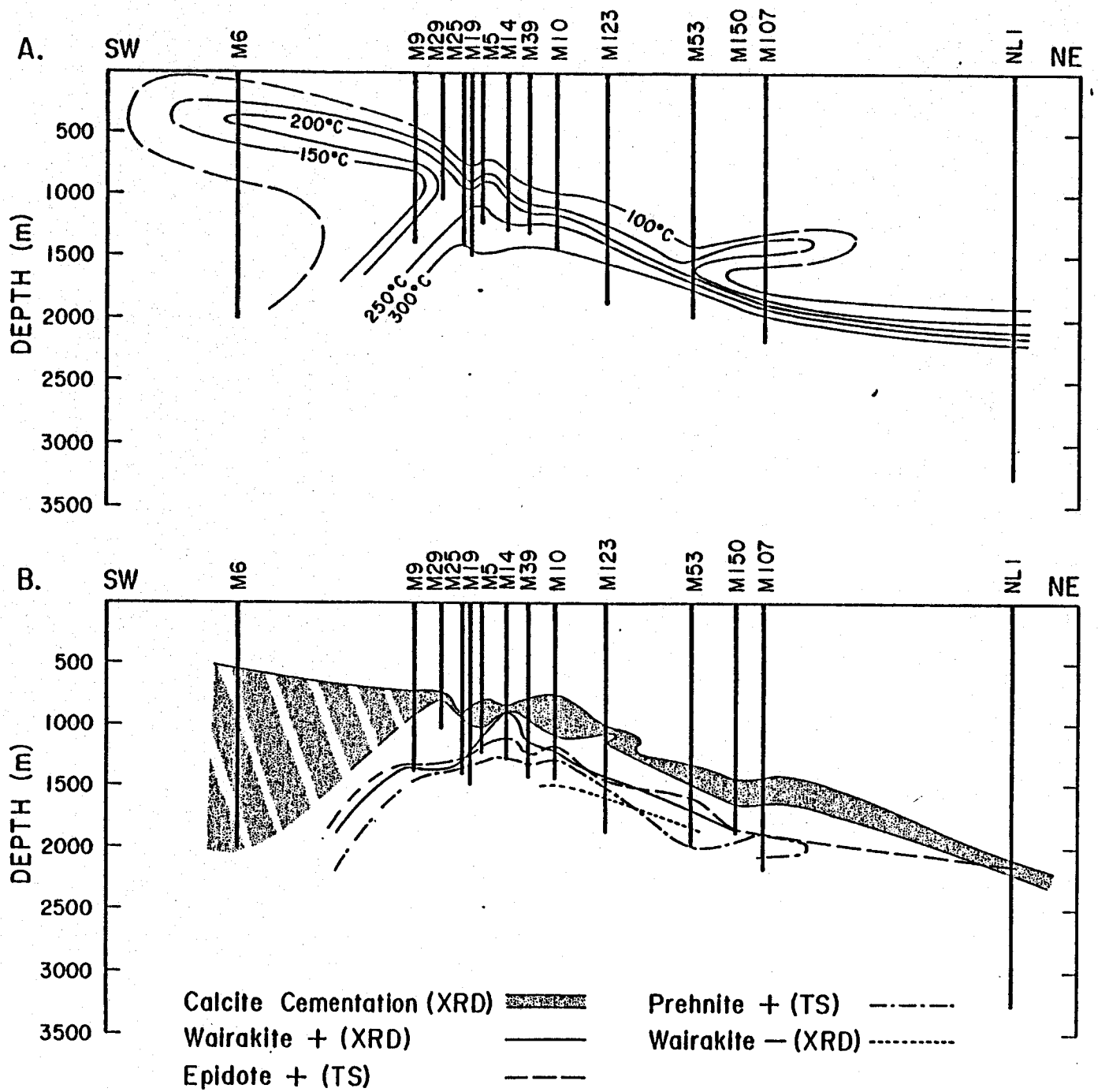
A.
SW
M6
M9
M29
M25
M19
M5
M14
M39
M10
M123
M53
M150
M107
NL1
NE
200°C
150°C
100°C
250°C
300°C
DEPTH (m)
500
1000
1500
2000
2500
3000
3500
B.
SW
M6
M9
M29
M25
M19
M5
M14
M39
M10
M123
M53
M150
M107
NL1
NE
DEPTH (m)
500
1000
1500
2000
2500
3000
3500
Calcite Cementation (XRD)
Wairakite + (XRD)
Epidote + (TS)
Prehnite + (TS)
Wairakite — (XRD)

Figure 13.

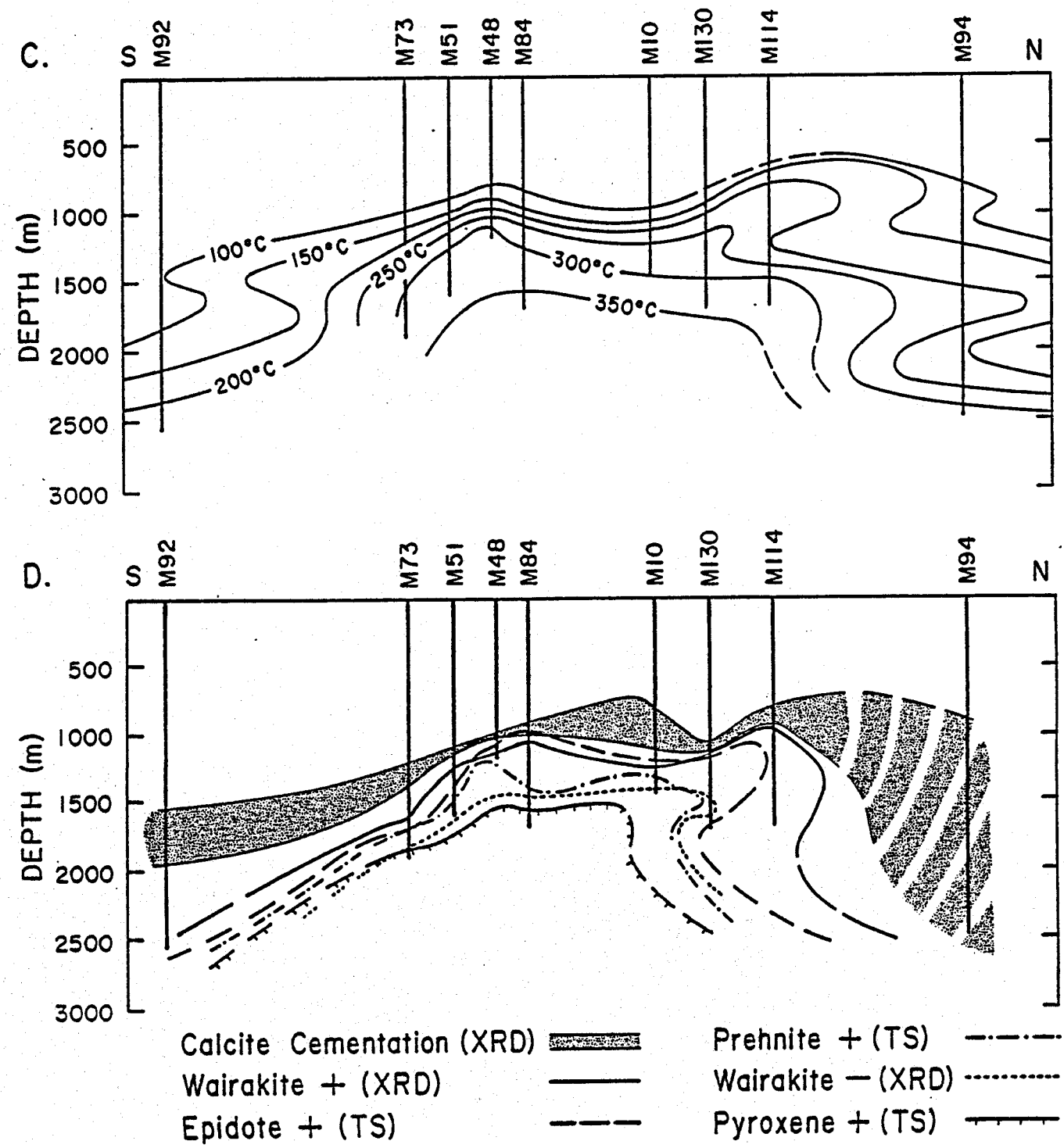
C.
S
M92
M73
M51
M48
M84
M10
M130
M114
M94
N
DEPTH (m)
500
1000
1500
2000
2500
3000
100°C
150°C
200°C
250°C
300°C
350°C
D.
S
M92
M73
M51
M48
M84
M10
M130
M114
M94
N
DEPTH (m)
500
1000
1500
2000
2500
3000
Calcite Cementation (XRD)
Wairakite + (XRD)
Epidote + (TS)
Prehnite + (TS)
Wairakite — (XRD)
Pyroxene + (TS)

Figure 13.

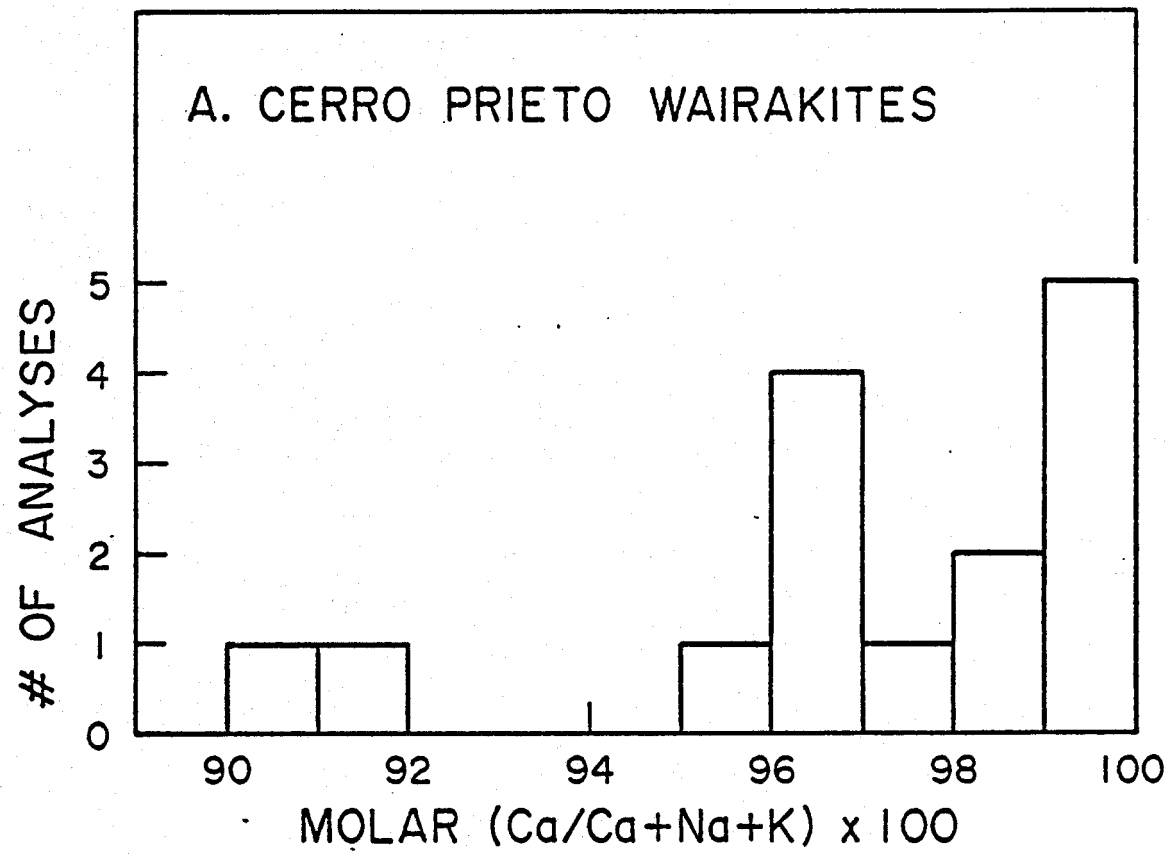
A. CERRO PRIETO WAIRAKITES
OF ANALYSES
0
1
2
3
4
5
90
92
94
96
98
100
MOLAR (Ca/Ca+Na+K) x 100

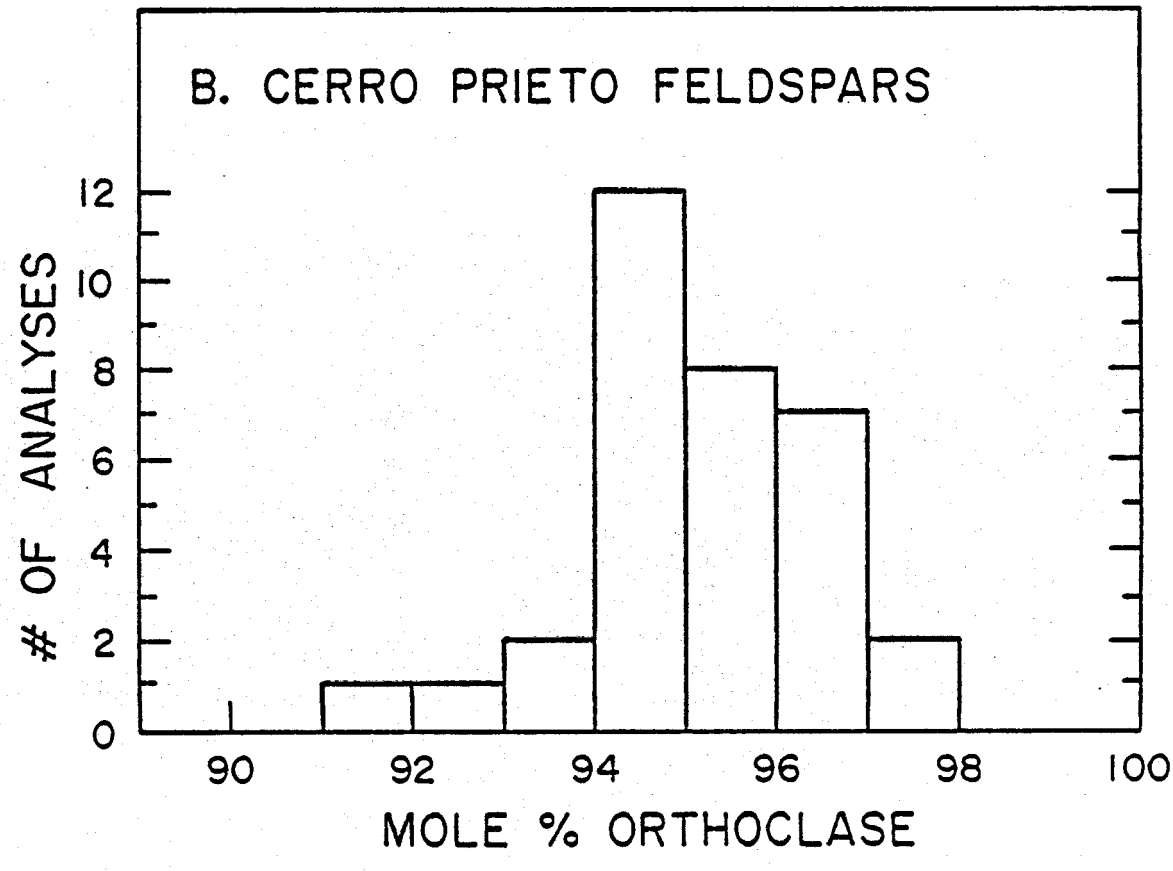
B. CERRO PRIETO FELDSPARS
OF ANALYSES
0
2
4
6
8
10
12
90
92
94
96
98
100
MOLE % ORTHOCLASE

Figure 14.

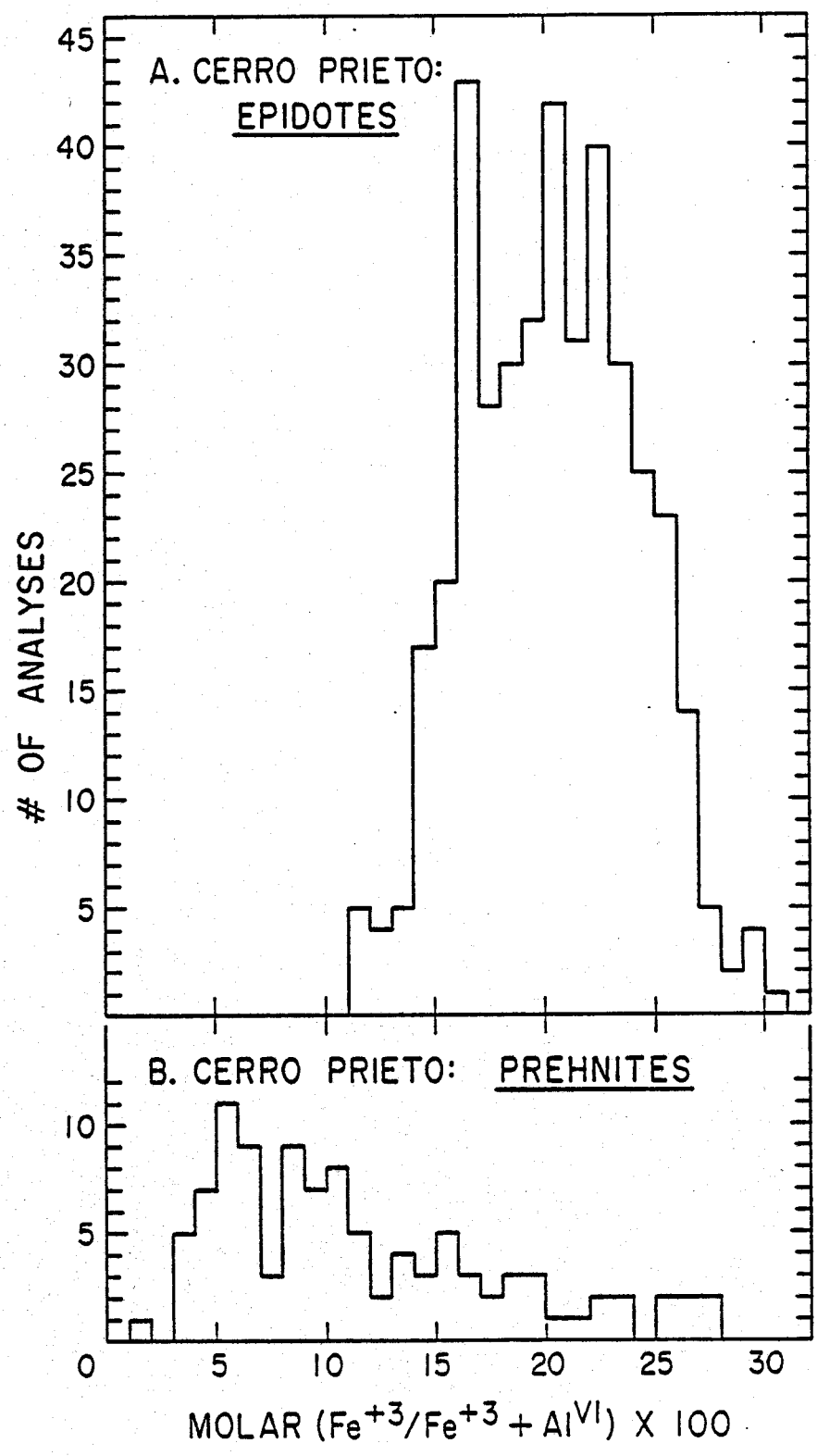
A. CERRO PRIETO:
EPIDOTES
B. CERRO PRIETO: PREHNITES
OF ANALYSES
MOLAR (Fe+3/Fe+3 + AlVI) X 100
0
5
10
15
20
25
30
35
40
45

Figure 15.

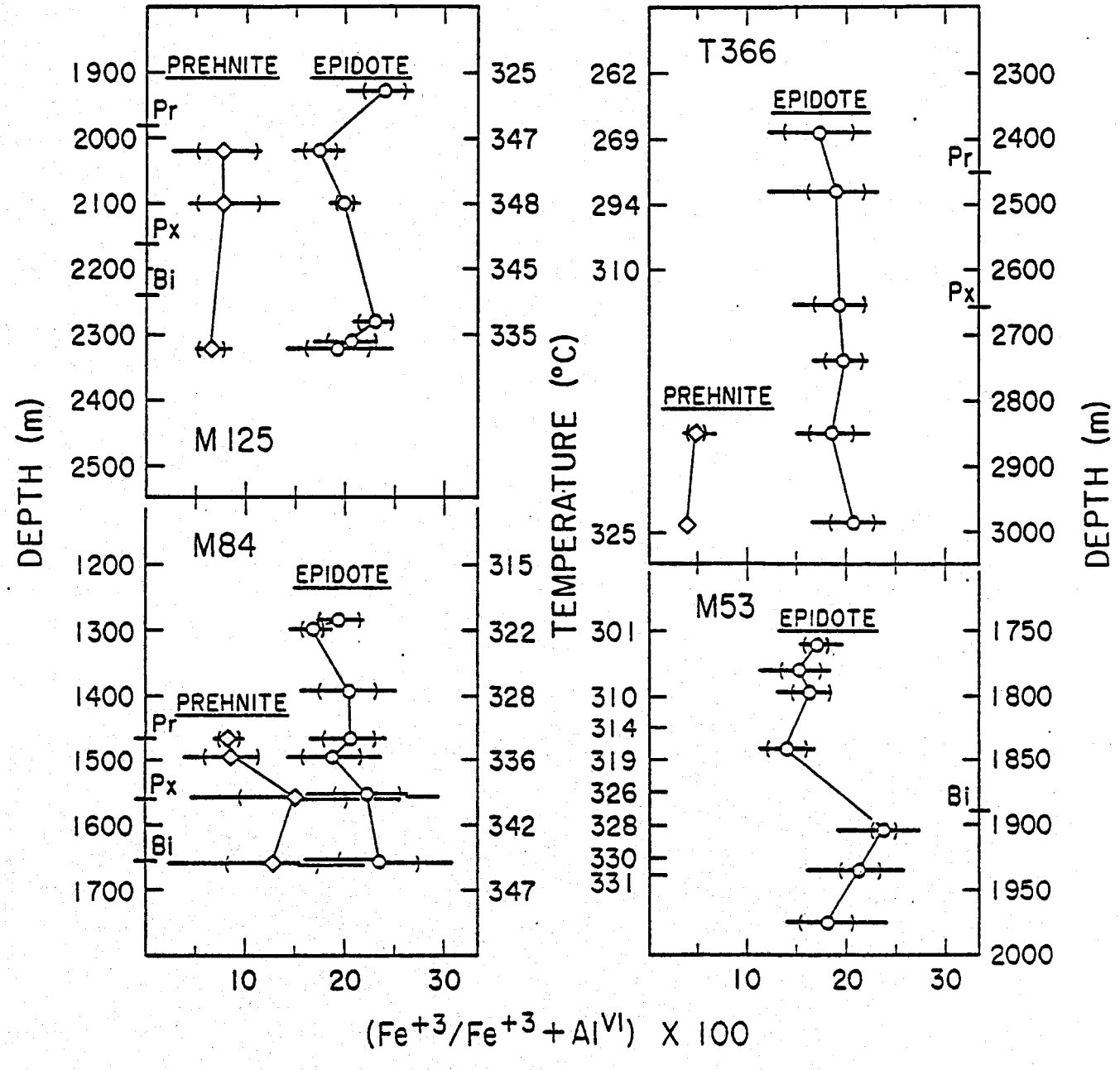
M125
PREHNITE
EPIDOTE
Pr
Px
Bi
1900
2000
2100
2200
2300
2400
2500
325
347
348
345
335
M84
EPIDOTE
PREHNITE
1200
1300
1400
1500
1600
1700
315
322
328
336
342
347
T366
EPIDOTE
PREHNITE
262
269
294
310
325
2300
2400
2500
2600
2700
2800
2900
3000
M53
EPIDOTE
301
310
314
319
326
328
330
331
1750
1800
1850
1900
1950
2000
DEPTH (m)
TEMPERATURE (°C)
10
20
30
(Fe+3/Fe+3+AlVI) X 100

Figure 16.

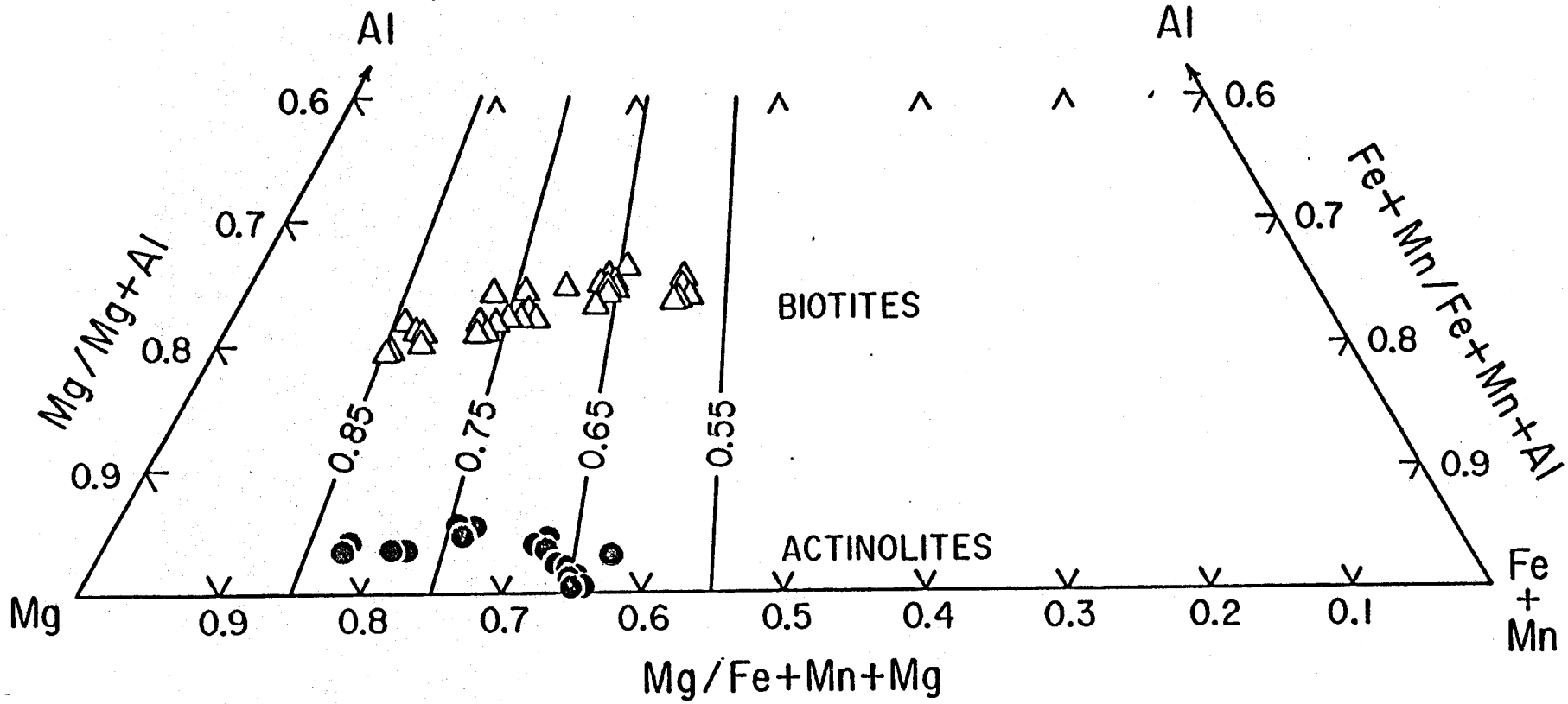
Al
0.6
0.7
0.8
0.9
Mg/Mg+Al
0.85
0.75
0.65
0.55
BIOTITES
ACTINOLITES
Mg
0.9
0.8
0.7
0.6
0.5
0.4
0.3
0.2
0.1
Mg/Fe+Mn+Mg
Al
0.6
0.7
0.8
0.9
Fe+Mn/Fe+Mn+Al
Fe
+
Mn

Figure 17.

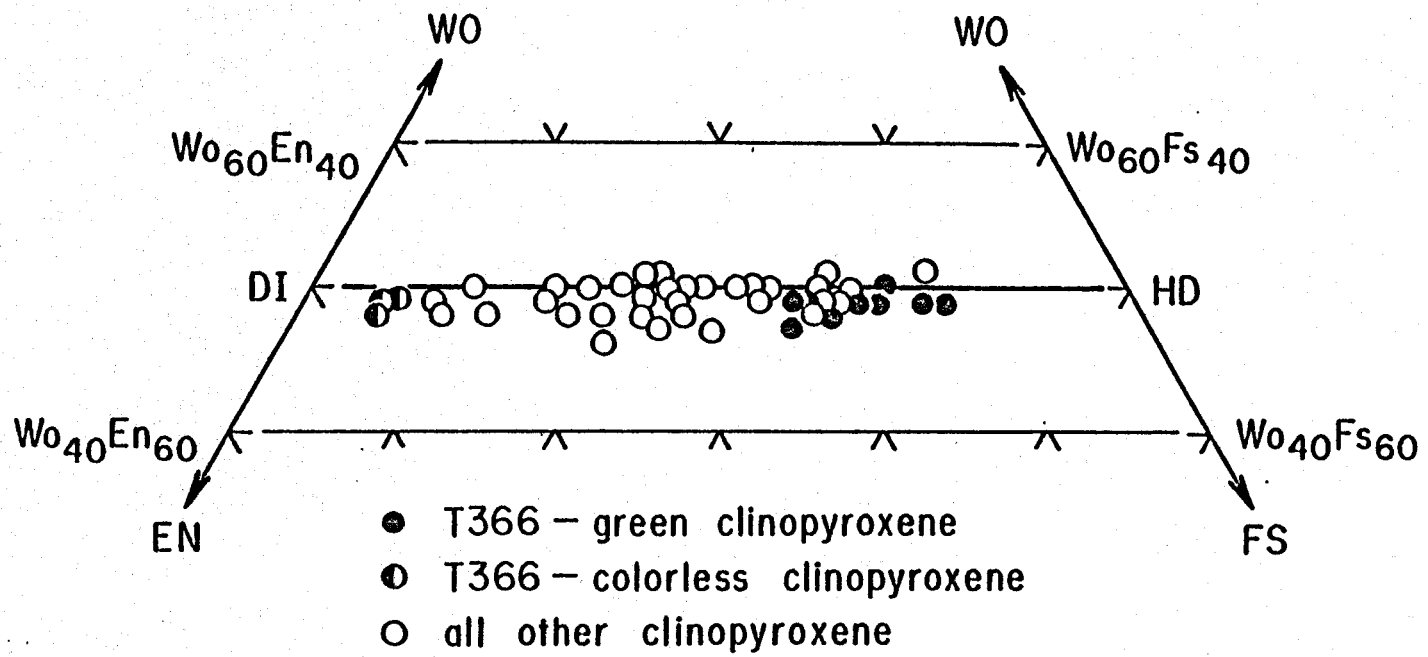
WO
WO
$Wo_{60}En_{40}$
$Wo_{60}Fs_{40}$
DI
HD
$Wo_{40}En_{60}$
$Wo_{40}Fs_{60}$
EN
FS
T366 – green clinopyroxene
T366 – colorless clinopyroxene
all other clinopyroxene

Figure 18.

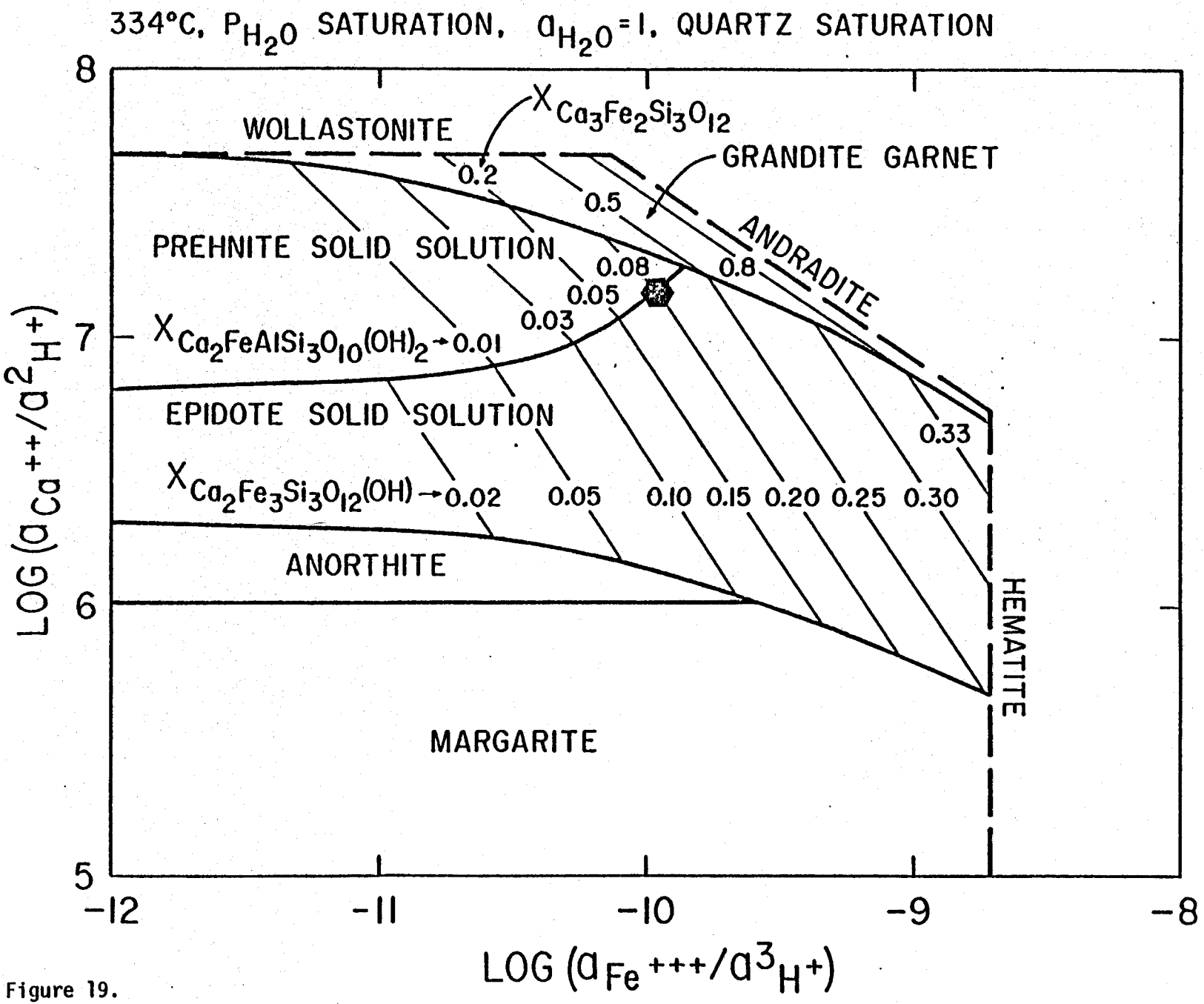
334°C, P_{H_2O} SATURATION, a_{H_2O}=1, QUARTZ SATURATION
WOLLASTONITE
$X_{Ca_3Fe_2Si_3O_{12}}$
GRANDITE GARNET
ANDRADITE
PREHNITE SOLID SOLUTION
$X_{Ca_2FeAlSi_3O_{10}(OH)_2}$
EPIDOTE SOLID SOLUTION
$X_{Ca_2Fe_3Si_3O_{12}(OH)}$
ANORTHITE
MARGARITE
HEMATITE
0.2
0.5
0.8
0.08
0.05
0.03
0.01
0.33
0.02
0.05
0.10
0.15
0.20
0.25
0.30
8
7
6
5
-12
-11
-10
-9
-8
LOG ($a_{Ca^{++}}/a^2_{H^+}$)
LOG ($a_{Fe^{+++}}/a^3_{H^+}$)

Figure 19.

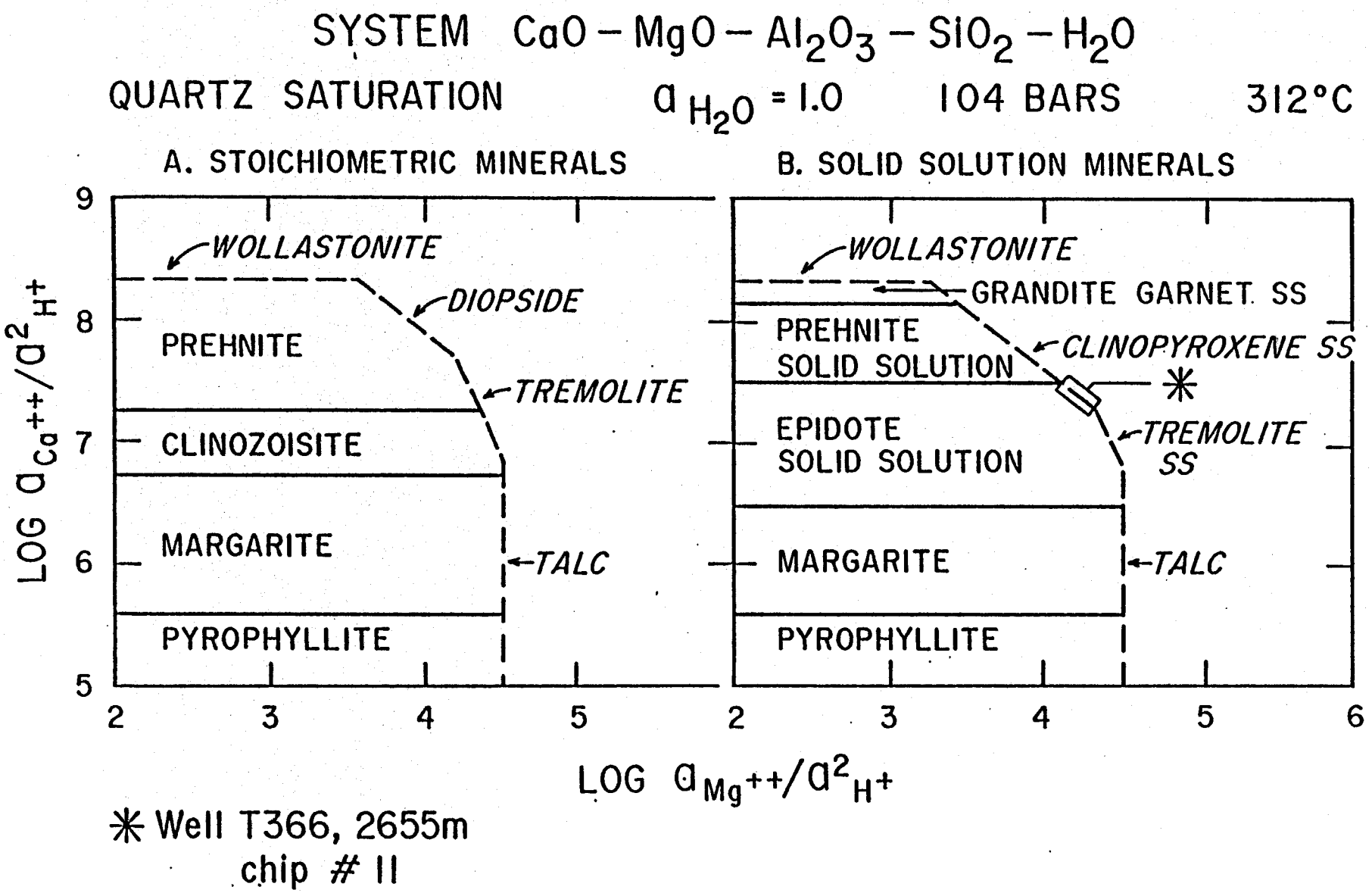
SYSTEM CaO – MgO – Al2O3 – SiO2 – H2O
QUARTZ SATURATION
a H2O = 1.0
104 BARS
312°C
A. STOICHIOMETRIC MINERALS
B. SOLID SOLUTION MINERALS
WOLLASTONITE
DIOPSIDE
PREHNITE
TREMOLITE
CLINOZOISITE
MARGARITE
TALC
PYROPHYLLITE
GRANDITE GARNET SS
PREHNITE SOLID SOLUTION
CLINOPYROXENE SS
EPIDOTE SOLID SOLUTION
TREMOLITE SS
LOG a Ca++/a2 H+
LOG a Mg++/a2 H+
9
8
7
6
5
2
3
4
5
6
* Well T366, 2655m
chip # 11

Figure 20.

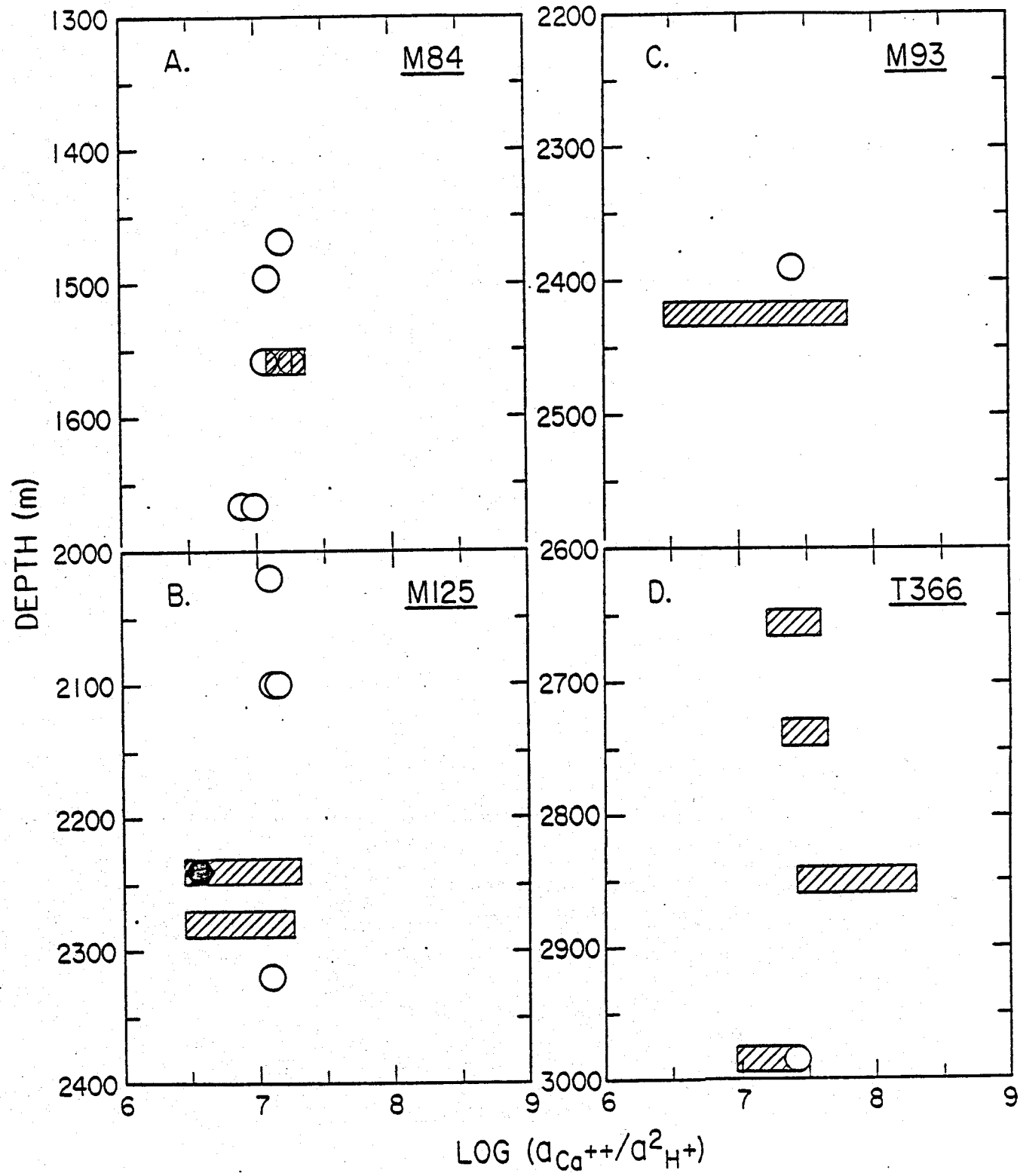
A.
M84
B.
M125
C.
M93
D.
T366
DEPTH (m)
1300
1400
1500
1600
2000
2100
2200
2300
2400
2200
2300
2400
2500
2600
2700
2800
2900
3000
6
7
8
9
LOG ($a_{Ca^{++}}/a^2_{H^+}$)

Figure 21.

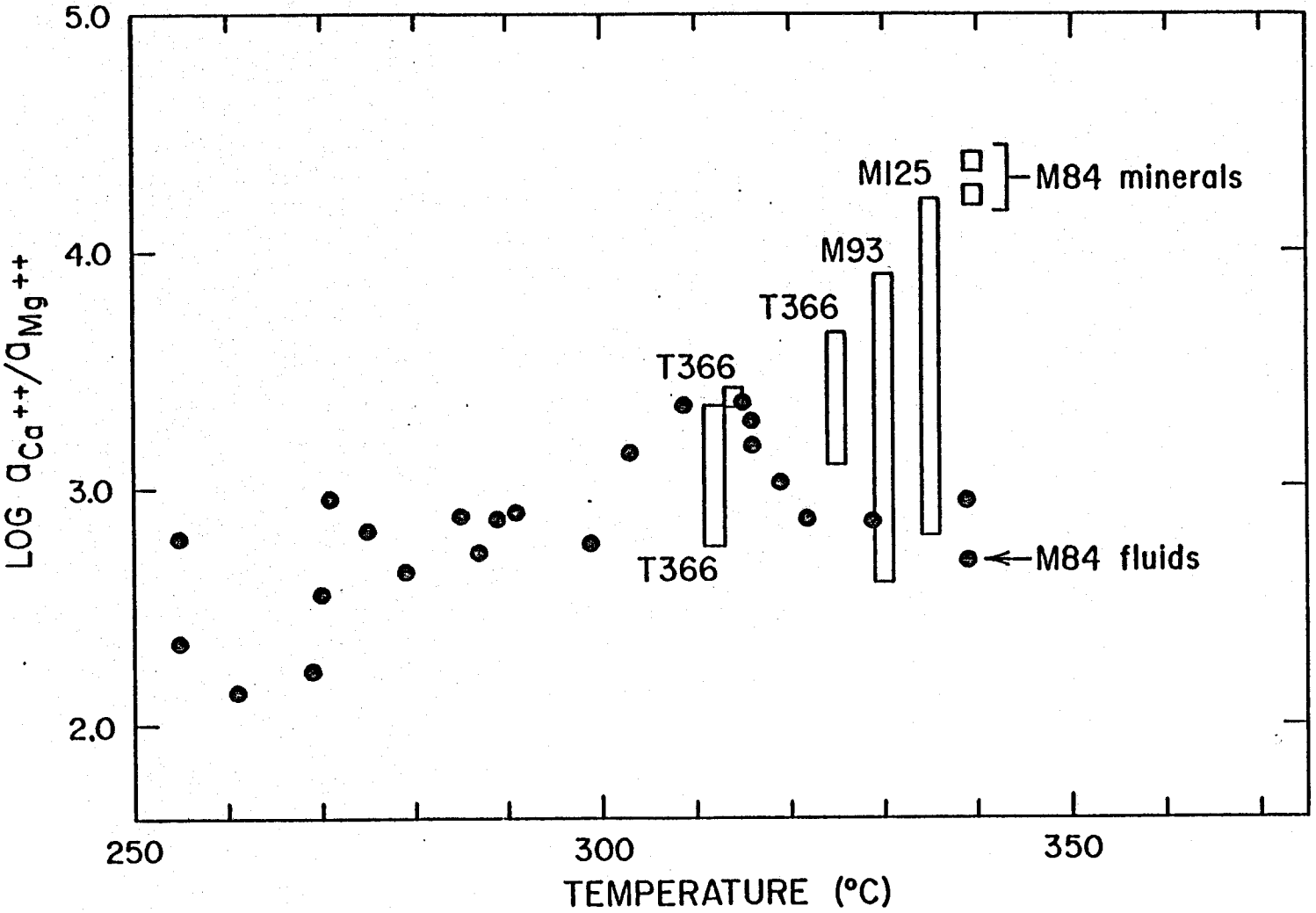
5.0
4.0
3.0
2.0
LOG $a_{Ca^{++}}/a_{Mg^{++}}$
250
300
350
TEMPERATURE (°C)
M125
M84 minerals
M93
T366
T366
T366
M84 fluids

Figure 22A.

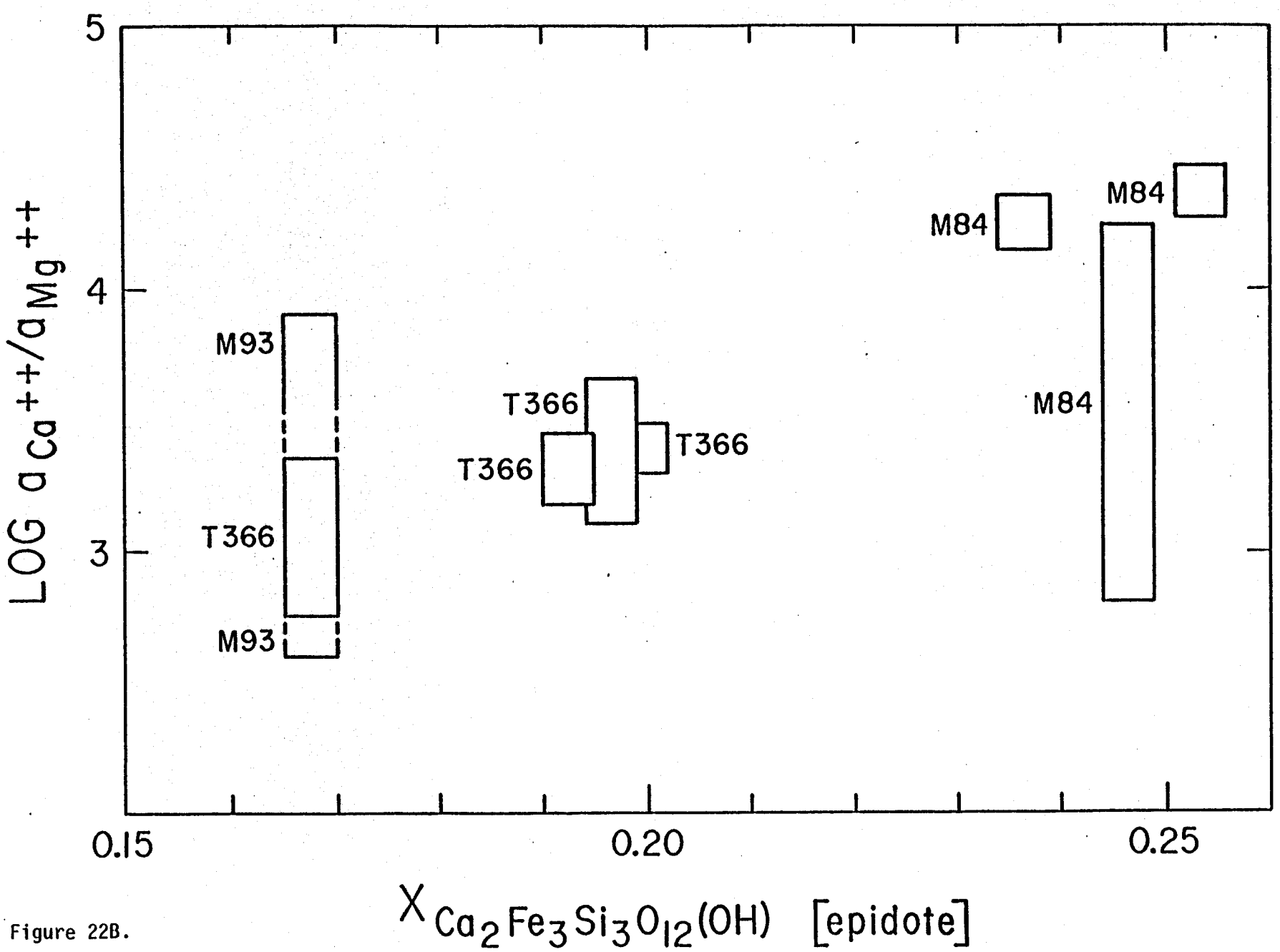
5
4
3
LOG $a_{Ca^{++}}/a_{Mg^{++}}$
M93
T366
M93
T366
T366
T366
M84
M84
M84
0.15
0.20
0.25
$X_{Ca_2Fe_3Si_3O_{12}(OH)}$ [epidote]

Figure 22B.

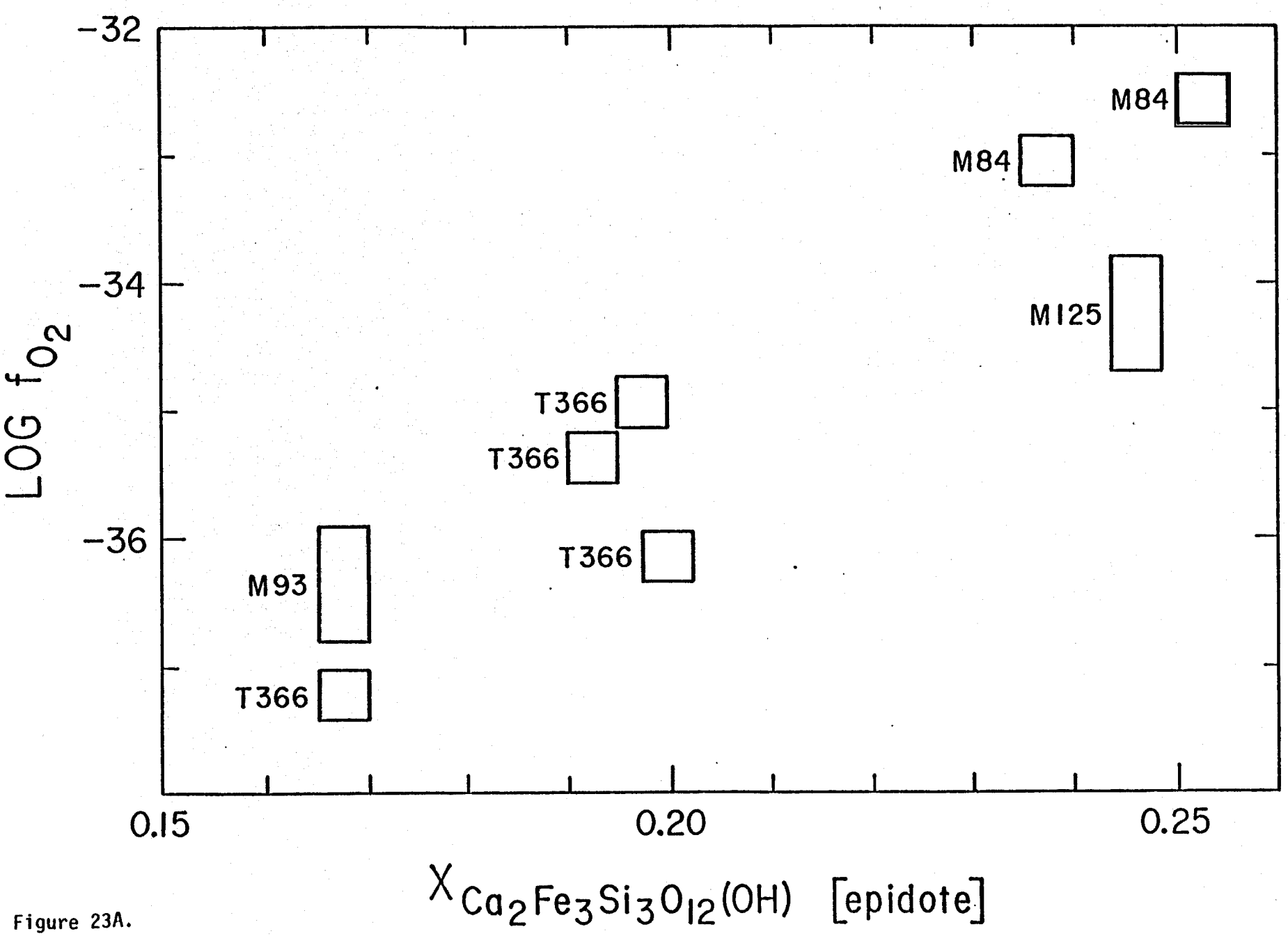
-32
-34
-36
LOG f_{O_2}
M84
M84
M125
T366
T366
T366
M93
T366
0.15
0.20
0.25
$X_{Ca_2Fe_3Si_3O_{12}(OH)}$ [epidote]

Figure 23A.

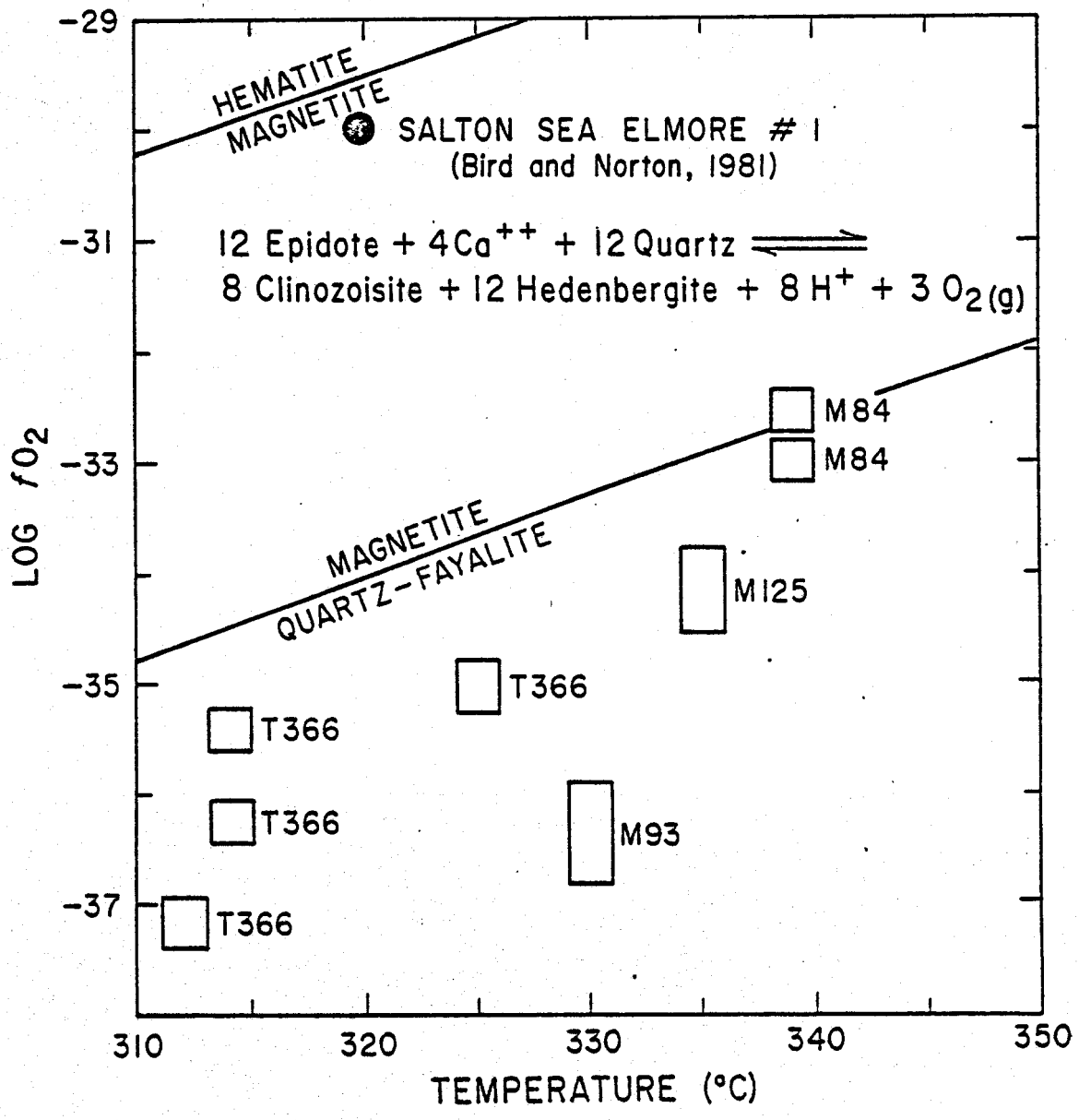
-29
-31
-33
-35
-37
LOG fO_2
HEMATITE
MAGNETITE
SALTON SEA ELMORE # 1
(Bird and Norton, 1981)
12 Epidote + 4 Ca^{++} + 12 Quartz ⇌
8 Clinozoisite + 12 Hedenbergite + 8 H^+ + 3 $O_{2(g)}$
M84
M84
MAGNETITE
QUARTZ-FAYALITE
M125
T366
T366
T366
M93
T366
310
320
330
340
350
TEMPERATURE (°C)

Figure 23B.